Catabolism of strigolactones by a carboxylesterase

Enjun Xu[1], Liang Chai[1,2], Shiqi Zhang[1,2], Ruixue Yu[1,2], Xixi Zhang[1,†], Chongyi Xu[1], Yuxin Hu[1,3*]

[1] Key Laboratory of Plant Molecular Physiology, CAS Center for Excellence in Molecular Plant Sciences, Institute of Botany, Chinese Academy of Sciences, Beijing, China.

[2] University of Chinese Academy of Sciences, Beijing, China.

[3] National Center for Plant Gene Research, Beijing, China. *e-mail: huyuxin@ibcas.ac.cn

[†] Present address: Institute of Science and Technology Austria (IST Austria), Am Campus 1, 3400 Klosterneuburg, Austria

Abstract

Strigolactones (SLs) are carotenoid-derived plant hormones that control shoot branching and communications between host plants and symbiotic fungi or root parasitic plants. Extensive studies have identified the key components participating in SL biosynthesis and signaling, whereas the catabolism or deactivation of endogenous SLs *in planta* remains largely unknown. Here we report that the *Arabidopsis* carboxylesterase 15 (AtCXE15) and its orthologues function as efficient hydrolases of SLs. We show that overexpression of *AtCXE15* promotes shoot branching by dampening SL-inhibited axillary bud outgrowth. We further demonstrate that AtCXE15 could bind and efficiently hydrolyze SLs both *in vitro* and *in planta*. We also provide evidence that AtCXE15 is capable to catalyze hydrolysis of diverse SL analogues and that such CXE15-dependent catabolism of SLs is evolutionarily conserved in seed plants. These results disclose a catalytic mechanism underlying homeostatic regulation of SLs in plants, which also provides a rational approach to spatial-temporally manipulate the endogenous SLs and thus architecture of crops and ornamental plants.

Introduction

Strigolactones (SLs) are carotenoid-derived plant hormones that play crucial roles in the regulation of plant branching, plant-fungi symbiosis and germination of root parasitic weeds[1-6]. In terrestrial plants, SLs are synthesized from the β-carotene and are structurally classified into two distinct groups: canonical and non-canonical SLs[7]. Canonical SLs have a characteristic tricyclic lactone (ABC ring) whereas the non-canonicals lack the conventional B, or C ring structure, which connect to a butenolide D-ring via an enol ether bridge that is essential for their biological activities[7]. SLs are perceived by the dual function receptor/hydrolase DWARF14 (D14)[3,6,8-13], which subsequently recruits MORE AXILLARY GROWTH2 (MAX2) F-box protein to target transcriptional repressor SMAX1-like proteins (SMXL6, SMXL7, and SMXL8)/DWARF53 for proteasome-mediated proteolysis[14-19], leading to expression of downstream transcription factor genes, such as *BRANCHED1*(*BRC1*)[20-23], to inhibit axillary bud outgrowth and thus shoot branching**.** The perturbation of SL biosynthesis or signaling results in the altered shoot branching and plant architecture. Thus, SLs are considered to be a class of shoot branching hormones, and manipulation of SL homeostasis or signaling has become a critical breeding target for crops and ornamental plants.

The SL receptor D14 is characterized as a member of α/β-fold hydrolase (ABH) superfamily and exhibits a weak hydrolysis activity towards SL[6,10]. The binding and hydrolysis of D14 toward SL had been considered to be necessary for SL signaling[8,15,24]. Intriguingly, a recent study argues that the binding rather than hydrolysis of SL by D14 is essential for SL signaling *in planta*[12]. Given the extremely low hydrolytic activity and rapid SL-dependent degradation of D14[9-11,25], it is likely that the SL hydrolysis by D14 may not represent a key mechanism behind catabolic regulation of endogenous SLs. In this study, we identified an evolutionarily conserved carboxylesterase that functions as an efficient hydrolase of SLs, which discloses a metabolic mechanism underlying the homeostatic regulation of SL in seed plants.

Results

Overexpression of *AtCXE15* promotes axillary bud outgrowth

In the transcriptomic profiling of auxin-induced cellular reprogramming in *Arabidopsis* regeneration, we noticed that transcription of the *carboxylesterase 15* (*AtCXE15*) was upregulated in root explants but downregulated in shoot explants upon callus-inducing medium (CIM) incubation (Extended Data Fig. 1a)[26]. To explore the possible function of AtCXE15 *in planta*, we overexpressed the *AtCXE15* in *Arabidopsis*, and surprisingly, the transgenic plants overexpressing *AtCXE15* (*AtCXE15-OE*) did not show any observed

phenotype in the callus-forming capacity but exhibited a striking hyperbranching phenotype, in which the number of rosette primary branches were correlated with the transcript and protein abundances of overexpressed AtCXE15 (Fig. 1a, b and Extended Data Fig. 1b). Given that the shoot branching in flowering plants is determined either by the initiation of axillary buds or by the outgrowth of dormant axillary buds[27], we further compared the number of formed axillary buds between wild-type (WT) and transgenic plants, and found that the equivalent axillary buds were formed in two genotypes (Fig. 1c), demonstrating that the excessive rosette primary branches in the transgenic *AtCXE15-OE* plants are due to the promotion of axillary bud outgrowth. However, an *AtCXE15* knockout mutant, *atcxe15-1*, and three *atcxe15* allelic mutants generated by CRISPR/Cas9, *atcxe15-2*, *atcxe15*-3 and *atcxe15-4*, displayed an indistinguishable shoot branching phenotype from WT plants (Fig. 1 and Extended Data Fig. 1c-e). As *Arabidopsis* CXE family contains 20 members, and phylogenetic analysis showed that AtCXE15 belongs to a unique clade distinct from other members (Extended Data Fig. 2a)[28], we attempted to investigate whether other AtCXE members might function redundantly with AtCXE15 in promoting shoot branching. Nevertheless, overexpression of other selected *AtCXE* genes in *Arabidopsis*, including two relatively close members *AtCXE6*, *AtCXE17*, the GA receptor subunit gene *GID1a*/*AtCXE10*, or *AtCXE2* and *AtCXE20* from other clades,

could not recapitulate the hyperbranching phenotype observed in *AtCXE15-OE* plants (Extended Data Fig. 2b, c)[29,30], implying that the other AtCXE members may not be involved in regulating shoot branching. These observations suggest that AtCXE15 functions distinctly from other AtCXE members in promoting axillary bud outgrowth.

AtCXE15 is involved in SL catabolism

Since SL play a central role in inhibiting axillary bud outgrowth, and *AtCXE15-OE* plants also resembled the *atd14-1* and SL biosynthetic mutant *atmax3-9* in the seedling morphology and compact leaf architecture (Extended Data Fig. 3a, b), we thus speculated that the excessive axillary bud outgrowth in *AtCXE15-OE* plants might be attributable to the impaired SL homeostasis or signaling. To test this, we first examined the transcriptomic profiling of *AtCXE15-OE*, *atd14-1*, and WT seedlings, and found that, among the 66 genes whose transcriptions were affected by overexpression of *AtCXE15*, more than 50% of these genes were also regulated in the *atd14-1* with a same transcriptional trend, including the SL biosynthetic genes *MORE AXILLARY GROWTH 3* (*AtMAX3*) and *AtMAX4*, whose transcriptions had a typical negative-feedback feature in SL signaling (Extended Data Fig. 3c, d and Supplementary Table 1)[31-37]. Next, we monitored the transcript levels of *AtMAX3* and the *AtBRC1*, a SL downstream target gene that inhibits axillary

bud outgrowth[20-23], in the axillary buds of *AtCXE15-OE* plants. As expected, similar to those observed in the SL biosynthetic mutant *atmax4-1* and signaling mutant *atmax2-1*, the transcript level of *AtMAX3* was significantly upregulated whereas the *AtBRC1* was remarkably downregulated in the axillary buds of *AtCXE15-OE* plants (Fig. 2a). Moreover, we also observed that transcript level of *AtCXE15* could be induced by the exogenous application of bioactive canonical SL (+)-GR24^{5DS} and non-canonical SL analogue methyl phenlactonoate 3 (MP3) at axillary bud region[38], where the transcription of *AtBRC1* was elevated upon application of (+)-GR24^{5DS} and (±)-MP3 (Fig. 2b). These observations strongly support that *AtCXE15* promotes axillary bud outgrowth in a SL-dependent manner.

The *AtCXE15* was widely expressed in multiple organs, including axillary buds, young leaves, hypocotyls, floral organs, and the vasculatures of shoots and roots, and AtCXE15 was found to be localized into cytosol and nucleus (Extended Data Fig. 4). As AtCXE15 and AtD14 belong to the ABH superfamily, we thus reasoned that the excessive axillary bud outgrowth in *AtCXE15-OE* plants might attribute to SL catabolism or impaired signaling. Indeed, unlike the SL biosynthetic mutants, whose hyperbranching can be rescued by grafting their shoots onto WT rootstocks[31,39,40], the hyperbranching phenotype of *AtCXE15-OE* were not restored by grafting an *AtCXE15-OE* shoot onto a WT root (Fig. 2c), excluding the possibility that the

hyperbranching phenotype in *AtCXE15-OE* plants is due to disturbed SL biosynthesis. As SLs and karrikins (KARs) have been reported to play a role in repressing hypocotyl elongation in an AtMAX2-dependent manner[41-44], while *AtCXE15-OE* seedlings did not mimic the elongated hypocotyl phenotype caused by mutation of the KAR receptor KARRIKIN INSENSITIVE2 (KAI2) (Extended Data Fig. 3b), we thus tested the hypocotyl response of the *atcxe15-1* and *AtCXE15-OE* seedling to exogenous (±)-GR24. The hypocotyl growth assay showed that *AtCXE15-OE* seedlings displayed a reduced sensitivity as did the *atd14-1*, however, the *atcxe15-1* seedlings were hypersensitive to exogenous (±)-GR24 (Fig. 2c), and such hypersensitivity of *atcxe15-1* hypocotyls to exogenous SL could be blocked by the disruption of *AtD14* (Fig. 2d), suggesting that AtCXE15 acts upstream of AtD14 and is not involved in SL signaling. Consistent with this, we failed to detect any interaction of AtCXE15 with well-known nuclear signaling components of SLs[14,16,17,19,25], including AtD14, AtMAX2 and AtSMXLs by IP-MS assay (Supplementary Table 2). To further examine the possible involvement of AtCXE15 in SL catabolism *in planta*, we further grafted the shoots of SL biosynthetic mutants, including *atmax3-9*, *atmax4-1* and *atmax1-1*[45-47], in which the SL biosynthetic pathway was disrupted at the synthetic step of 9-*cis*-β-apo-10'-carotenal, carlactone (CL), and carlactonoic acid (CLA), respectively (Fig. 2f)[37,48], on the *AtCXE15-OE* and *atcxe15-1* rootstocks. As

expected, when the SL biosynthetic mutants were grafted on *atcxe15-1* rootstocks, their hyperbranching phenotype was completely restored to that of WT (Fig. 2f). By contrast, grafting the *atmax3-9* shoots onto *AtCXE15-OE* rootstocks fully inhibited the excessive branches in *atmax3-9* shoots, whereas the excessive branching phenotype of *atmax4-1* and *atmax1-1* shoots were not completely rescued by grafting onto *AtCXE15-OE* rootstocks (Fig. 2f), demonstrating that the over-accumulation of AtCXE15 in *Arabidopsis* could result in the deficiency of endogenous potential non-canonical SLs CL, CLA, and/or methyl carlactonoate (MeCLA) and its derivatives rather than that of their upstream precursor 9-*cis*-β-apo-10'-carotenal, which might be potentially transmittable from the *AtCXE15-OE* rootstock into the *atmax3-9* shoot to form potential SLs. Taken together, we conclude that AtCXE15 participates in catabolism of SL *in planta*.

AtCXE15 is an efficient hydrolase of SL

To test whether AtCXE15 could hydrolyze SL, we first examined the binding activity of AtCXE15 to the non-canonical SL analogue (±)-MP3 and canonical SL (±)-5-Deoxystrigol (5DS). A label-free Microscale thermophoresis (MST) assay clearly showed that AtCXE15 had a high binding affinity to both (±)-MP3 and (±)-5DS (Extended Data Fig. 5a), demonstrating that AtCXE15 could bind to SLs. Next, we used a developed pro-fluorescent SL probe, Yoshimulactone

Green (YLG), whose fluorescence emission could be produced once hydrolyzed by AtD14[3], to examine the hydrolytic activity of AtCXE15. After the primary roots were incubated with YLG, the green fluorescent emission signals from the *AtCXE15-OE* roots were remarkably stronger than that from WT roots, while such fluorescence in the *atcxe15-1* roots was slightly weaker than that in WT roots (Fig. 3a), supporting that AtCXE15 could hydrolyze YLG *in planta*. Next, we assayed the *in vitro* hydrolytic activity of AtCXE15 and AtD14 toward YLG, and observed that, when YLG concentration was increased, the intensity of fluorescence produced by AtCXE15 was remarkably higher than that by AtD14, however, replacement of the third catalytic glutamate residue in the AtCXE15 (AtCXE15^{E271A}) abolished its hydrolytic activity toward YLG (Fig. 3b). Further real-time monitoring of fluorescent emissions confirmed that the hydrolytic activity of AtCXE15 toward YLG was much higher than that of AtD14 (Extended Data Fig. 5b), and the fluorescent signals produced by AtCXE15 or AtD14 could be attenuated by non-fluorescent SL (±)-GR24 in a dose-dependent manner (Extended Data Fig. 5c). By contrast, either AtCXE18 or AtCXE10/AtGID1a, which is known as an active esterase or gibberellins receptor without esterase activity, respectively[49,50], showed poor hydrolytic activity toward YLG, although an active esterase activity was detected in AtCXE18 (Extended Data Fig. 5b, d). These observations strongly suggest that AtCXE15 could efficiently hydrolyze SLs both *in vitro* and *in planta*.

To further validate the hydrolytic activity of AtCXE15 toward SL, we used KAR_1 as the internal standard and carried out an ultraperformance liquid chromatography tandem mass spectrometry (UPLC-MS) analysis after incubation of the (+)-GR24^{5DS} and (±)-MP3 with AtCXE15 and AtD14. Consistent with the high hydrolytic activity of AtCXE15 toward YLG, all the (+)-GR24^{5DS} and 95.7% of (±)-MP3 substrates were hydrolyzed by AtCXE15 after one hour incubation, whereas only less than 5% of (+)-GR24^{5DS} and (±)-MP3 were hydrolyzed by AtD14 at the same timepoint (Fig. 3c, d). Meanwhile, the hydrolysis product ABC-FTL (ABC-formyltricyclic lactone) corresponding to ABC-ring produced by AtD14 were highly detectable after incubation of AtCXE15 with (+)-GR24^{5DS}, confirming that AtCXE15 could cleave the enol ether bridge between ABC-ring and D-ring of (+)-GR24^{5DS} as did AtD14 (Fig. 3c)[6,8,10,12]. However, we could not detect any enriched hydrolysate from hydrolyzed (±)-MP3 either by AtCXE15 or AtD14 (Fig. 3d), which might be due to other ester bond present in (±)-MP3 or poor stability of hydrolysates.

Since the diverse canonical and non-canonical SLs have been characterized in different plant species[7,51,52], we further investigated whether AtCXE15 could hydrolyze different SL analogues. As expected, when AtCXE15 was incubated with various SL analogues, including the orobanchol-type SL (±)-orobanchol, (-)-2'-*epi*-GR24^{4DO}, and the strigol-type SL

(±)-5DS, the hydrolytic activity of AtCXE15 and the product corresponding to ABC-ring were also highly detected (Fig. 4a-c). Since MeCLA is considered to be a likely bioactive SL in *Arabidopsis* and is extremely unstable under *in vitro* condition[53-56], we performed the assay by intermediately diluting the freshly synthetic MeCLA and incubating with AtCXE15 and AtD14 proteins. Consistently, we observed that all the MeCLA substrate was hydrolyzed by AtCXE15 whereas less than 3% of substrate was hydrolyzed by AtD14 after 10 min incubation (Fig. 4d). Collectively, these results demonstrate that AtCXE15 could target and hydrolyze the diverse types of SLs.

CXE-mediated SL catabolism is conserved in seed plants

The *CXE* gene family exists widely in plant kingdom and plays an important role in the breakdown and recycling of cellular metabolites[28,49,57]. To explore whether CXE15-mediated SL catabolism is conserved *in planta*, we firstly conducted the best protein BLAST homology searches using AtCXE15 amino acid sequence and attempted to identify the putative AtCXE15 orthologues from three dicots species (*Brassica napus* L.*, Medicago truncatula*, *Glycine max* L.), one monocot species (*Oryza sativa subsp. Japonica*), one Gymnosperms species (*Dioon edule* from *Cycadales*), and one bryophytes species (*Physcomitrium patens*). All the putative AtCXE15 orthologues from Gymnosperms and Angiosperms but moss were clustered together (Fig. 5a

244 and Extended Data Fig. 6a). Next, we tested the hydrolytic activity of these
245 AtCXE15 orthologues toward YLG. Intriguingly, the putative AtCXE15
246 orthologues from three dicot, one monocot and one Gymnosperms species
247 showed a strong hydrolytic activity toward YLG (Fig. 5b), whereas the putative
248 AtCXE15 orthologue PpCXE3 from *Physcomitrium patens* showed poor
249 hydrolytic activity toward YLG (Fig. 5b). As the origin of SL coincides with the
250 emergence of primitive land plants including moss lineage[51,58-60], we further
251 tested the hydrolytic activity of other four PpCXEs members towards YLG, and
252 found that none of them showed hydrolytic activity (Extended Data Fig. 6b). In
253 addition, the transcription of *AtCXE15* orthologues in rice and *B. napus* L.,
254 *OsCXE17* and *BnaCXE15*, were found to be induced by exogenous (±)-GR24
255 (Extended Data Fig. 6c). To further examine possible conservation of
256 CXE15-mediated SL catabolism *in planta*, we generated the transgenic
257 *Arabidopsis* plants overexpressing *BnaCXE15*, *MtCXE15*, *GmCXE15*,
258 *OsCXE17*, *DeCXE15*, or *PpCXE3*, respectively. Consistent with the hydrolysis
259 activities toward YLG, overexpression of the *BnaCXE15*, *MtCXE15*,
260 *GmCXE15*, *OsCXE17*, or *DeCXE15* but not the *PpCXE3* in *Arabidopsis*
261 resulted in the hyperbranching phenotype (Fig. 5c and Extended Data Fig. 6d),
262 demonstrating that CXE15-mediated SL catabolism is at least evolutionarily
263 conserved in seed plants. Interestingly, we also noticed that the canonical
264 catalytic triad of Ser/His/Asp residues for ABH family in the CXE15

orthologues of Gymnosperms and monocots, was substituted by Ser/His/Glu residues in dicots (Fig. 5a), implying that CXE15 orthologues in dicots might have undergone some degree of evolutionary divergence from their ancestors. Therefore, the CXE15-dependent catabolism of SLs likely emerges from Gymnosperms or ancestor of seed plants.

Discussion

As a newly identified plant hormone that plays a key role in inhibiting shoot branching, SL biosynthesis and signaling have been extensively documented in terrestrial plants[1,6,13-15,17,37,40,48,51,58,61], whereas little is yet known about how SLs are deactivated at the catabolic level. This might be largely due to the very low abundance of SLs and their biosynthesis under a strict feedback regulation in plants[32-36]. Here, we identified the *Arabidopsis* AtCXE15 as a functional SL hydrolase, and our further works revealed that CXE15-mediated SL catabolism is evolutionarily conserved in seed plants. This discloses an unidentified catabolic mechanism underlying SL homeostatic regulation in plants. Although D14 has been reported to be the non-recyclable receptor with hydrolytic activity toward SLs[6,8,10,12], the extremely weak hydrolytic activity and rapidly SL-dependent degradation suggest that D14 is not likely a core catalytic enzyme for the spatial-temporal regulation of SL gradients *in planta*[9,10]. However, as the strict feedback regulation of SL biosynthesis has

been reported *in planta* and the abundant accumulation of endogenous SLs does not result in an obvious shoot branching phenotype[32-36,48,62], it might be why disruption of AtCXE15 does not obviously affect the shoot branching. Moreover, the SL biosynthetic or signaling mutants have been reported to be hypersensitive to biotic/abiotic stresses[63-66], while the transcription of important genes involved SL biosynthesis and signaling, such as *AtD14*, *AtMAX2*, and *AtMAX3*, does not appear to be effectively responsive to biotic/abiotic stresses (Extended Data Fig. 7)[65,66]. By contrast, the transcription of *AtCXE15* seems to be highly responsive to SL, auxin and various environmental cues, including pathogenic elicitors flg22 and HrpZ, ozone, salt stress, and drought stress (Fig. 2b, Extended Data Fig.1a, Extended Data Fig. 6c and Extended Data Fig. 7). Therefore, it is also likely that the CXE-mediated SL catabolism represents a mechanism to precisely balance SLs within plant organs to respond to ever-changing environments.

Since CXEs belong to an ABH superfamily that function as carboxylic ester hydrolase of both xenobiotics and endogenous metabolites in plants[67], the catalytic specificity of AtCXE15 orthologues or paralogues on SLs remains to be further determined. Indeed, although our work reveals that the AtCXE15 and its orthologues in some species function as efficient SL hydrolases, it does not exclude the possibility that some other ABH members might be also involved in this process, because we only selected the representative ACXE15

orthologues by their amino acid similarity to AtCXE15. On the other hand, AtCXE15 could bind and hydrolyze both canonical and non-canonical SLs, and our grafting assay clearly demonstrate that such catabolic reaction mediated by CXE15 also occurs with CL, CLA, and MeCLA (Fig. 2f), which are known to be potential SLs[37,48,61]. Furthermore, given that CXE15-dependent catabolism of SLs is conserved in seed plants, an interesting question raised is whether such regulation co-evolves with the emergence of SL molecules. We now know that the CL is present in bryophyte *Physcomitrium patens*[7,58,68], but the actual receptor in the moss is yet unknown[59,60]. Therefore, further investigation will be helpful to clarify whether CXE15-dependent SL degradation is coincided with the appearance of SL or signaling.

Finally, SLs are synthesized in both basal part of shoots and roots and are transportable acropetally[1,51], implying that the local gradient of SLs within specific organ such as axillary buds and roots is essential for its biological function in shoot branch development and fungi-plant interactions, respectively. Our grafting data showed that overexpression of *AtCXE15* in shoot alone is sufficient to trigger hyperbranching, demonstrating that CXE15 can coordinate the SL level at specific locales. Thus, manipulation of local SL gradients by *CXE15* orthologues under a tissue-specific or inducible promoter will be a powerful approach to differentiate their roles in plant development and its interaction with fungi and root parasitic plants, which has a great potential in

shaping the architecture of crops and ornamental plants and avoiding the adverse effect caused by noxious root parasitic plants.

Methods

Plant materials and growth conditions

The *Arabidopsis* Columbia accession Columbia-0 (Col-0) was used as wild type in all experiments. The *atcxe15-1* (Salk_203698c) seeds were obtained from the *Arabidopsis* Biological Resource Center (ABRC). The *kai2-2* (Col-0), *atmax3-9*, *atmax4-1*, *atd14-1*, and *atmax2-1* mutants were described previously[45-47,69,70]. Seeds of *Arabidopsis* and *B. napus* L. were sterilized with 75% ethanol containing 2% Triton X100, stratified in darkness at 4°C for three days, and germinated on 1/2 Murashige and Skoog (MS) medium. The seedlings and plants were grown in the growth chamber at 22°C with a 16-h-light/8-h-dark photoperiod and an illumination intensity of 80-90 mmol $m^{-2}s^{-1}$. The rice (*O. sativa japonica*, Nipponbare) seedlings were grown on Yoshida medium in the growth chamber at 30°C with same photoperiod and illumination intensity described above.

SL Chemicals and treatment assays

The SL analogues (±)-5DS, (±)-orobanchol, (+)-$GR24^{5DS}$, and (-)-2'-*epi*-$GR24^{4DO}$ were purchased from Strigolab (Italy), (±)-GR24 was

purchased from YEASEN Biotech (China), KAR_1 was purchased from TRC (Canada), and YLG was purchased from TCI AMERICA, respectively. The methyl phenlactonoate 3 (MP3) and methyl carlactonoate (MeCLA) were synthesized by chemical reactions using the strategies described previously[38,53,54,71]. The synthesized (±)-MP3 and MeCLA were verified by LC-MS and ^{1}H NMR (Supplementary Fig.1). As MeCLA is highly unstable[53-55], the freshly synthetic MeCLA purified from *prep*-HPLC was diluted immediately to perform the hydrolysis assay. All other SL analogues were dissolved in dimethylsulfoxide (DMSO) to create a 10 mM stock solution. For gene expression analyses, the aerial parts of four-week-old plants were submerged in 1 μM (+)-GR24^{5DS} or (±)-MP3 at 22℃ for 3 h, and the axillary tissues were collected for RNA isolation. The 11-day-old *Arabidopsis*, *B. napus* L., and rice seedlings treated with 5 μM (±)-GR24 for 3 h were used to monitor the transcript abundance of *AtCXE15* orthologues. For hypocotyl growth assay[8], the seedlings grown on 1/2 MS medium supplemented with 0, 0.1, 0.5, 1, 3, 5 and 10 μM (±)-GR24 at 22℃ under continuous low light for nine days were photographed, and hypocotyl length was quantified using ImageJ software (https://imagej.nih.gov/ij).

Plasmid construction and plant transformation

The In-Fusion cloning based on *in vitro* homologous recombination was performed to generate all the constructs using an In-Fusion HD Cloning Kit (Clontech) and Hieff Clone® Plus Multi One Step Cloning Kit (Yeasen, Shanghai). The allelic mutants *atcxe15-2, atcxe15-3*, and *atcxe15-4* were generated by using the egg cell-specific promoter-controlled CRISPR/Cas9 system as previously described[72]. For *in vitro* protein assay, the coding sequences of *AtD14*, *AtCXEs*, and *AtCXE15* putative orthologues were retrieved from the Ensembl Plants database and 'onekp database v5'[73], and then cloned into the pGEX-4T-2 plasmid or pET-28a-c (+) plasmid to generate glutathione S-transferase (GST)-tagged proteins or His-tagged *AtCXE15* (Clontech), respectively. Meanwhile, a mutagenized AtCXE15^{E271A} construct lacking enzymatic activity was also generated by substitution of third catalytic glutamate residue with alanine residue. To generate transgenic *Arabidopsis* plants, the CXE15 paralogues or putative orthologues were cloned into the pSUPER1300 vector[74]. The *AtCXE15* with or without GFP-tagged constructs were also generated in pSUPER1300-GFP vector or pVIP96 vector, respectively[75]. To examine the expression and subcellular localization of AtCXE15, a 2 kb promoter region of *AtCXE15* fused with upstream of the β-glucuronidase (GUS) gene and a 2 kb promoter fused with coding region of *AtCXE15* were cloned into the pCAMBIA1300 or pCAMBIA1300-GFP vector, respectively. All the resulted constructs were verified by sequencing and

introduced into *Agrobacterium tumefaciens* strain EHA105 or ABI and transformed into Col-0 plants by the standard floral dipping method[76]. All the primers and their restriction enzyme sites used for constructs are listed in in Supplementary Table 3.

Gene expression

Total RNAs were isolated using E.Z.N.A.® Plant RNA Kit according to the manufacturer's instructions (OMEGA Bio-TEK). The qRT-PCR, RNA-sequencing analysis, and GUS histochemical assay were performed as previously described[77,78]. The software FastQC (0.11.7), HISAT2 (2.1.0), Picard-tools (version 1.41), Samtools (version 0.1.18), RStudio (version 1.3.1073), and DESeq (version 1.39.0) were used in RNA-seq analysis. The primers used are shown in Supplementary Table 3.

AtCXE15 subcellular localization

For subcellular localization of AtCXE15, ten-day-old transgenic *pCXE15:CXE15:GFP* seedlings were immersed in 1% sucrose medium supplemented with 1 μg/mL FM4-64 (Invitrogen) and vacuum for 3 min. Fluorescence images were acquired by ZEISS LSM 980 with Airyscan 2 laser scanning confocal microscope. Filter settings were as follows: excitation (488

nm), emission (509 nm), detection for eGFP (490-525 nm), and for FM4-64 (650-757 nm).

Grafting assay

Seven-day-old seedlings were used for the grafting assay following the protocol described previously[79]. Each combination of scion and rootstock was grafted at least 11 times, and the representative plants were photographed.

Protein expression and purification

The recombinant GST-tagged or His-tagged proteins were purified with Glutathione Sepharose beads or Ni-NTA agarose beads according to the manufacturer's instruction (GE Healthcare), respectively. The beads were eluted as previously described[80]. The eluted protein was concentrated using Pierce™ protein concentrators (Thermo Fisher) and then diluted with 1X PBS buffer (pH=7.3) and concentrated for buffer exchange at least six times. The purified protein was adjusted to 5 μg/μL. The protein solution was aliquoted and immediately frozen in liquid nitrogen and stored at -80°C until use.

Microscale thermophoresis (MST) assay.

The 0.5 μM AtCXE15-GST protein in 1X PBS buffer (pH=7.3) was mixed at a 1:1 ratio respectively with 16 different concentrations of (±)-5DS and (±)-MP3

in 1X PBS containing 10% DMSO (ranging from 0.000763 to 25 μM). About 10 μl of each sample was loaded into a hydrophobic monolith NT capillary (NanoTemper Technologies). Thermophoresis was monitored at 25°C in a Monolith NT. Label Free instrument at a constant LED power of 20% and MST power of 40%. The K_d values were determined by plotting the concentrations of (±)-5DS or (±)-MP3 against the changes in thermophoresis signal, and the data were analyzed with MO.Affinity Analysis v2.2.7 software. Experiments were performed repeatedly on independent protein preparations to ensure reproducibility (n>5).

YLG hydrolysis assay

YLG hydrolysis assay was conducted with 0.2 μM of recombinant GST-tagged proteins in 1X PBS reaction buffer (pH 7.3). YLG was diluted in reaction buffer to give a concentration gradient of 2-22 μM. The proteins and dilution of YLG were mixed in a 96-well plate in a 100 μL final volume. The measurements were performed on a BioTek Synergy MX microplate reader at 37°C using 480 nm excitation and a 520 nm emission wavelength. The fluorescence intensity was measured after 40 min incubation. The background signal generated by YLG degradation in the mock reaction at each concentration (2-22 μM) was subtracted, and the normalized intensity was then converted to fluorescein concentration by comparing to fluorescent intensity of complete hydrolysis of 1

μM YLG. The hydrolysis kinetics analysis of YLG was performed using 0.02 μM of recombinant proteins in 1X PBS reaction buffer (pH 7.3) supplemented with 1 μM YLG at a 50 μl volume on a 96-well plate under ice-cold temperature. The mixes of CXE protein and YLG were covered with sealing foils, and the fluorescence intensity was immediately measured by LightCycler® 96 Real-Time PCR System using an excitation wavelength of 470 nm and a detection wavelength of 512 nm. For the (±)-GR24 competition assay, 1 μM YLG was pre-mixed with (±)-GR24 with serial dilutions range from 1 μM to100 μM before AtCXE15 or AtD14 protein was added. Time-course YLG hydrolysis was monitored at 37°C for 35-45 min. DMSO was added in equivalent concentration into each reaction. The absolute fluorescence values were converted to fluorescein concentration by normalizing to fluorescent intensity of complete hydrolysis of 1 μM YLG.

The YLG hydrolysis in *planta* was performed with the primary roots of six-day-old *AtCXE15-OE*, *atcxe15-1* and WT seedlings incubated with 1 μM YLG for three minutes. Fluorescence images were acquired with an Olympus SZX7 fluorescent Olympus Stereo Microscope, and the green fluorescence was quantified by ImageJ software.

SL analogue hydrolysis assay

The SLs or their analogues (100 μM) were incubated with or without 1 μM purified AtCXE15-GST and AtD14-GST for 1 or 4 h at 37°C in PBS buffer (1 mL, pH=7.4, 5% DMSO). The 200 ul of solution was taken from same reaction at each timepoint and immediately mixed up with 800 μl of ice-cold acetone and incubated at -20°C for 2 h. The proteins were pelleted at 13,000g at 4°C for 20 min, and the supernatants were subjected to a reverse-phase, Ultra high pressure liquid chromatography quadrupole time-of-flight mass spectrometer (UHPLC/Q-TOF-MS, Agilent 1290/6540) at a flow rate of 0.4 mL/min. The retention time of various SLs and their hydrolysis ABC ring (ABC-formyltricyclic lactone, ABC-FTL) were monitored as following: the intact (+)-GR24^{5DS} and ABC-FTL were eluted at 11.2 and 7.6 min; the intact (-)-2'-*epi*-GR24^{4DO} and ABC-FTL were eluted at 11.2 and 7.6 min; intact (±)-5DS and ABC-FTL were at 14.8 and 11.8 min; intact (±)-orobanchol and ABC-FTL were at 10.3 and 7.4 min; the intact (±)-MP3 and its stereoisomer molecule were at 11 and 11.2 min; and intact MeCLA was eluted at 18.2 min, respectively. The 100 μM KAR_1 was added to each reaction as internal standard, and intact KAR_1 was eluted at 5.3 min. The corresponding ABC-FTL product and remaining substrate were analyzed, and their peak areas were normalized with KAR_1 to calculate for relative hydrolytic activities of AtCXE15 and AtD14. The data were analyzed by MassHunter Qualitative Analysis software (Agilent, version B.04.00).

Enzymatic assay with 4-nitrophenyl acetate (4-NPA)

Esterase activities of AtCXEs and AtD14 against 4-NPA were determined by measuring the amount of 4-nitrophenol released by esterase-catalyzed hydrolysis. The 100 μM 4-NPA was incubated with 1 μM purified protein for 30 min at 37°C in 1X PBS buffer (pH=7.3, 5% DMSO). The product 4-nitrophenol was monitored in 5-min intervals up to 30 min at 405 nm by use of a Nano-300|Micro Spectrophotometer.

Phylogenetic analysis

The *Arabidopsis AtCXEs* and rice *OsCXEs* have been described previously[28], Sequences of CXE families of *Physcomitrium patens*, *B. napus* L., *Medicago truncatula*, and *Glycine max* L. were collected using the AtCXE15 protein sequence as a query to search against Ensembl Plants database by HmmerWeb version 2.41.1 (https://www.ebi.ac.uk/Tools/hmmer/), with default settings. The putative CXE15 amino acid sequences of *Dioon edule* were collected by the best-BLASTP match searches in the 'onekp database v5' from The 1000 Plant Transcriptomes Project (https://db.cngb.org/blast/blast/blastp/)(One Thousand Plant Transcriptomes Initiative, 2019)[73]. The CXE amino acid sequences of various species were aligned using MUSCLE (version 3.8.31). Phylogenetic analysis of 20 AtCXEs and/or AtCXE15 putative orthologues was performed using the Mega X

514 software (Maximum Likelihood method, bootstrap method with 1,000 iterations,
515 Jones-Taylor-Thornton (JTT) model, uniform rates among sites, complete
516 deletion of gaps/missing data, Nearest-Neighbor-Interchange (NNI) method).
517
518 **Statistical analysis**
519 For gene-expression analyses, observations of phenotype, and statistical
520 analysis were assessed as described in the figure legends. *p* and *F* (degree of
521 freedom) values were calculated by two-tailed Student's *t*-tests and one-way
522 ANOVA using Prism 8.0 software, respectively. No statistical methods were
523 used to predetermine sample size. The experiments were not randomized.
524
525 **Data availability**
526 The RNA-seq data is deposited in the Gene Expression Omnibus
527 (www.ncbi.nlm.nih.gov/geo/) under the accession number GSE176007.
528 Sequence data from this article can be found in Ensembl Plants
529 (http://plants.ensembl.org/index.html) or 'onekp database v5'
530 (https://db.cngb.org/blast/blast/blastp/), under the following accession
531 numbers: *AtCXE1*(AT1G19190.1), *AtCXE2* (AT1G47480.1), *AtCXE3*
532 (AT1G49640.1), *AtCXE4* (AT1G49650.1), *AtCXE5* (AT1G49660.1), *AtCXE6*
533 (AT1G68620.1), *AtCXE7* (AT2G03550.1), *AtCXE8* (AT2G45600.1), *AtCXE9*
534 (AT2G45610.1), *AtCXE10* (AT3G05120.1), *AtCXE11* (AT3G27320.1),

AtCXE12 (AT3G48690.1), *AtCXE13* (AT3G48700.1), *AtCXE14* (AT3G63010.1), *AtCXE15*(AT5G06570.1), *AtCXE16* (AT5G14310.1), *AtCXE17* (AT5G16080.1), *AtCXE18* (AT5G23530.1), *AtCXE19* (AT5G27320.1), *AtCXE20* (AT5G62180.1), *AtD14* (AT3G03990.1), *AtMAX3* (AT2G44990.1), *AtMAX4* (AT4G32810.1), *AtSMXL6* (AT1G07200.1), *AtSMXL7* (AT2G29970.1), *AtSMXL8* (AT2G40130.1), *AtMAX2* (AT2G42620.1), *AtBRC1* (AT3G18550.1), *OsCXE17* (Os07g0162700-01), *PpCXE2* (Pp3c3_16760V3.1), *PpCXE3* (Pp3c5_13820V3.1), *PpCXE5* (Pp3c12_10130V3.1), *PpCXE6* (Pp3c13_21400V3.1), *PpCXE8* (Pp3c18_20160V3.1), *GmCXE15* (GLYMA_19G202900/KRG96320), *BnaCXE15* (BnaC09g48990D-1), *MtCXE15* (MTR_7g107040/KEH24302), *DeCXE15* (gnl|onekp|WLIC_scaffold_2120524). All reagents and materials are available from the corresponding author upon request. Source data are provided with this paper.

Acknowledgements

We thank J. Li (Institute of Genetics and Developmental Biology, China) for providing the *at14-1*, *atmax2-1*, *atmax3-9*, *atmax4-1, atmax1-1, kai2-2* (Col-0 background) mutants, and B. Xu for providing the cDNA of *Physcomitrium patens*. We are grateful for L. Wang for assistance to MST, B. Han for assistance to UPLC-MS, J. Li for assistance to confocal microscopy, and B.

Mikael and J. Zhang for their comments on the manuscript. This work was supported by the grants from Strategic Priority Research Program of Chinese Academy of Sciences (Y.H.: XDB27030102) and the National Natural Science Foundation of China (E.X.: 31700253, Y.H.: 31830055).

Author contributions

E.X. and Y.H. design the overall research. E.X. carried out most of the experiments. L.C., S.Z., R.Y. X.Z., and C.X. contributed to the plasmid construction, generation of transgenic plants, shoot branching assay, and RNA-seq analysis. E.X. and Y.H. analyzed the data and wrote the manuscript.

Competing interests

The authors declare no competing interests.

Additional information

Extended data is available for this paper.

Supplementary information is available for this paper.

Materials & Correspondence should be addressed to Y.H.

Figure legends

Fig. 1| Overexpression of *AtCXE15* stimulates shoot branching. a, Representative shoot branching phenotype of wild type (Col-0), *atcxe15-1*, and three independent transgenic *AtCXE15-OE* lines. Arrow indicates primary rosette branches; Scale bar, 1cm. **b**, Primary rosette branch number (upper panel) and transcript abundance of *AtCXE15* (bottom panel) in the plants described above. The mean branch numbers are shown as black lines. n = 3 biological replicates of 16 plants for each genotype. The qRT-PCR data were normalized to the Col-0 and are shown as means ± s.d.; *F* (degree of freedom) values are shown; The letters in **b** indicate statistical differences between genotypes determined by one-way ANOVA followed by Tukey's honestly significant difference (HSD) test for multiple comparisons ($P<0.05$). **c**, Diagram of the axillary bud positions in Col-0, *atcxe15-1* and three independent transgenic *AtCXE15-OE* lines. Each row represents an individual plant, and each square represents one leaf (n = 7). The green and orange squares represent the rosette leaves with and without axillary bud, respectively.

Fig. 2| AtCXE15 is involved in catabolism of SLs. a, Transcript abundance of *AtMAX3* and *AtBRC1* in the axillary region of Col-0, *AtCXE15-OE*, *atmax2-1*, *atmax4-1* plants. Data were normalized to the Col-0 and are shown as means ± s.d.; n = 3 biological replicates. **b**, Transcriptional response of *AtCXE15* to

canonical SL (+)-GR24^{5DS} and non-canonical SL (±)-MP3. Transcript abundances of *AtCXE15* and *AtBRC1* were monitored in the axillary tissue of four-week-old Col-0 plants after treatment with1 μM (+)-GR24^{5DS} or (±)-MP3 for 3 h. Data were normalized to the mock and are shown as means ± s.d.; n = 3 biological replicates. **c**, Hypocotyl length of Col-0, *atcxe15-1*, *atmax2-1*, *atd14-1* and *AtCXE15-OE* seedlings treated with (±)-GR24. Seedlings were grown on 1/2 MS medium supplemented with 0, 0.1, 0.5, 1, 3, 5 and 10 μM (±)-GR24 for nine days. Data are shown as means ± s.d.; n = 3 biological replicates of at least 12 seedlings. **d**, Hypocotyl length of Col-0, *atcxe15-1*, *atd14-1*, and *atd14-1 atcxe15-1* seedlings treated with (±)-GR24. Seedlings were grown on 1/2 MS medium supplemented with 0.5 μM (±)-GR24 for nine days under low light growth conditions. Data are shown as means ± s.d.; n = 5 biological replicates of at least 15 seedlings. **e**, Branching phenotype (upper panel) and the primary rosette branch number (bottom panel) in the grafted Col-0 and *AtCXE15-OE* plants. Data are shown as means ± s.d.; n = 11-13 grafted plants. Scale bar, 1cm. **f**, The grafting assay with SL biosynthetic mutants and *AtCXE15-OE* or *atcxe15-1* plants. A proposed SL biosynthetic pathway in *Arabidopsis* is shown in upper panel[55,56], in which the potential non-canonical SLs are indicated as laurel-green background. The primary rosette branch number in five-week-old grafted plants is shown in bottom panel. Data are shown as means ± s.d.; n = 14. Note that only the excessive

branches in the *atmax3-9* scion were completely rescued by *AtCXE15-OE* rootstocks. The mean branch numbers are shown as black lines **e** and **f**. *P* values are shown in **c**; two-tailed Student's *t*-test. *F* (degree of freedom) values are shown; The letters in **a**, **b**, **d**, **e**, **f** indicate statistical differences between genotypes determined by one-way ANOVA followed by Tukey's HSD test for multiple comparisons (P<0.05).

Fig. 3| AtCXE15 can bind and efficiently hydrolyze SLs. a, Hydrolytic activity of AtCXE15 toward YLG in *planta*. Representative fluorescence image photographed from Col-0, *AtCXE15-OE* and *atcxe15-1* primary roots treated with 1 μM YLG for three minutes and their relative green fluorescence are shown in left panel and right panel, respectively. The red dotted box indicates fragment of primary roots (about 2 cm from transition zone) selected for quantification of green fluorescence. Scale bar, 0.5 cm; Data were normalized to that of Col-0. Bars are means of relative fluorescence; n = 11-12 seedlings. **b**, Hydrolysis of AtCXE15 and AtD14 toward different concentrations of YLG *in vitro*. The green fluorescent signals were monitored after 40 min incubation of 0.2 μM protein. Background signals at each concentration of YLG were subtracted from the reaction buffer with proteins and converted to fluorescein/μM. Note that AtD14 exhibits much weaker enzymatic activity compared to AtCXE15 and enzymatic activity in the AtCXE15^{E271A} is abolished.

638 Data are means ± s.d.; n = 6 technical replicates. **c**, **d**, Hydrolytic activity of
639 AtCXE15 and AtD14 toward (+)-GR24^{5DS} and (±)-MP3 assayed by
640 UHPLC/Q-TOF-MS. The intact (+)-GR24^{5DS} and (±)-MP3, and the
641 corresponding hydrolytic products were monitored in a positive mode, and the
642 peak areas were calculated for relative hydrolytic activities of AtCXE15 and
643 AtD14; The two peaks of (±)-MP3 ligand were verified by LC-MS and NMR and
644 confirmed that they were (+)-MP3 and its stereoisomer (**d**); The 100 μM KAR_1
645 was added to each solution as internal standard. *P* values are shown in **a**;
646 two-tailed Student's *t*-test. The experiment was repeated at least two times
647 independently with similar results.
648
649 **Fig. 4| Hydrolytic activity of AtCXE15 toward SL analogues. a-c**, Hydrolytic
650 activity of AtCXE15 toward canonical SLs (-)-2'-*epi*-GR24^{4DO}, (±)-5DS, and
651 (±)-orobanchol. The intact (-)-2'-*epi*-GR24^{4DO} and ABC-FTL were eluted at
652 11.2 and 7.6 min (**a**), intact (±)-5DS and ABC-FTL were eluted at 14.8 and
653 11.8 min (**b**), and intact (±)-orobanchol and ABC-FTL were eluted at 10.3 and
654 7.4 min (**c**), respectively. **d**, Hydrolytic activity of AtCXE15 and AtD14 toward
655 non-canonical SL MeCLA. The synthetic MeCLA purified by *prep*-HPLC was
656 immediately diluted to 25 μM and incubated with and without AtCXE15/AtD14
657 in PBS buffer for 10 min. The intact MeCLA was eluted at 18.2 min. The 100

μM KAR_1 was added to each solution as an internal standard. The experiment was repeated at least two times independently with similar results.

Fig. 5| CXE15-mediated SL catabolism is conserved in seed plants. a, Phylogeny of the putative AtCXE15 orthologues from indicated dicots, monocots, gymnosperm, and bryophytes species. Numbers are percent bootstrap values for 1,000 replicates. AtD14 was used as outgroup. The third amino acid residue of catalytic triad is highlighted in red. **b**, YLG hydrolytic activities of putative AtCXE15 orthologues described above. Data are means ± s.d.; n = 3 technical replicates. **c**, The primary rosette branch number of transgenic *Arabidopsis* plants overexpressing *BnaCXE15*, *MtCXE15*, *OsCXE17*, *GmCXE15*, *DeCXE15* and *PpCXE3*, respectively. Each data point indicates the number of primary rosette branches from each independent transgenic plant. **d**, Proposed model for evolutionary history of CXE15-mediated SLs catabolism. The black arrow indicates the lineages of extant plants in the order they appear. The origin of SLs catabolism and perception likely coincides with the emergence in seed plants. It remains unknown whether SLs catabolism is conserved in early land plants.

Extended Data Fig. 1| Characterization of *AtCXE15-OE* plants and *atcxe15* mutants. a, Transcript abundance of *AtCXE15* in the shoot and root explants upon CIM treatments. Log_2-transformed relative transcript values of AtCXE15 is calculated by comparing transcript level of *AtCXE15* at each time points to 0 h. Magenta, green and white indicate upregulation, downregulation, and no change, respectively. **b**, Characterization of *AtCXE15-OE* plants carrying a *p35S*:*AtCXE15*:*GFP* construct. The primary rosette branch number, transcript abundance of *AtCXE15*, and AtCXE15-GFP and Actin protein levels in the corresponding transgenic plants are shown from upper to bottom panels, respectively. The GFP-tagged AtCXE15 and endogenous Actin levels were detected by immunoblotting with a monoclonal anti-GFP and anti-actin antibody, respectively; the dilution rate for both antibodies is 1: 2,000. **c**, Molecular characterization of the T-DNA insertion mutant *atcxe15-1*. The T-DNA insertion site and positions of the primers used RT-PCR are indicated by black triangles and red lines, respectively. The experiment was repeated at least two times independently with similar results. **d**, The mutations in *atcxe15* alleles generated by the CRISPR/Cas9 system. The CRISPR/Cas9 targeting sites on *AtCXE15* are shown in blue letters followed by red protospacer adjacent motif (PAM), and allelic mutations in the *atcxe15-2*, *atcxe15-3*, and *atcxe15-4* are shown as indicated. **e**, Quantified rosette primary shoot branch number in the three *atcxe15* plants described above. The means of branch

number are shown as black lines in **b** and **e**; n = 3 biological replicates of 10 plants for each genotype. The qRT-PCR data were normalized to the Col-0 and are shown as means ± s.d. in **b**; n = 4 biological replicates of 16 plants for each genotype. The statistical analysis was performed by comparing Col-0 with each *AtCXE15-OE* line or *atcxe15* genotype; *F* (degree of freedom) values are shown; The letters in **b** and **e** indicate statistical differences between genotypes determined by one-way ANOVA followed by Tukey's HSD test for multiple comparisons ($P<0.05$).

Extended Data Fig. 2| Characterization of AtCXEs in shoot branching regulation. a, Phylogeny of AtCXE members. Numbers are percent bootstrap values for 1,000 replicates. AtCXEs highlighted in green are selected for generation of the transgenic plants. **b**, Morphology of five-week-old transgenic plants overexpressing the *AtCXE2*, *AtCXE6*, *AtCXE10*, *AtCXE16*, *AtCXE17*, or *AtCXE20*, respectively. Bars = 1 cm. **c**, The primary rosette branch number (upper panel) and transcript abundance of *AtCXEs* (bottom panel) in the transgenic plants described above. Three independent transgenic lines for each genotype were characterized, and the means of branch number are shown as black lines. n = 3 biological replicates of 10 plants for each genotype. The qRT-PCR data were normalized to the Col-0 and are shown as means ± s.d.; n = 3 biological replicates from 10 plants for each independent line. The

statistical analysis was performed by comparing Col-0 with each *AtCXE-OE* genotype; *F* (degree of freedom) values are shown; The letters in **c** indicate statistical differences between *AtCXE* transgenic plants determined by one-way ANOVA followed by Tukey's HSD test for multiple comparisons ($P<0.05$).

Extended Data Fig. 3| Morphology and transcriptome profiling of *AtCXE15-OE* plants. a, Morphology of the four-week-old Col-0, four allelic *atcxe15s*, *atd14-1*, *atmax3-9*, *kai2-2*, and three independent transgenic *AtCXE15-OE* plants. Scale bar, 1 cm. **b**, Hypocotyl phenotype of one-week-old Col-0, four allelic *atcxe15s*, *atd14-1*, *atmax3-9*, *kai2-2*, and three independent transgenic *AtCXE15-OE* seedlings. Data for each genotype are shown as means ± s.d.; n = 3 biological replicates of at least 15 seedlings. *F* (degree of freedom) values are shown; The letters above each bar indicate statistical differences between genotypes determined by one-way ANOVA followed by Tukey's HSD test for multiple comparisons ($P<0.05$). **c,** Overview of the differentially expressed genes (DEG) in the *atd14-1* and *AtCXE15-OE* vs Col-0 seedlings revealed by RNA-seq. The FDR < 0.05 and Log_2fold change >1 or Log_2fold change < -1; n = 3. **d**, Heatmap of the overlapping DEG in the *atd14-1* and *AtCXE15-OE*. Log_2-transformed relative expression values of genes is

shown. Magenta, green and white indicate upregulation, downregulation, and no change, respectively.

Extended Data Fig. 4| Tissue-specific expression of *AtCXE15* and subcellular localization of AtCXE15. a-e, GUS staining assayed seedling or organs of transgenic *Arabidopsis* plants carrying a *pAtCXE15*:*GUS* construct. Young seedling (a-c); primary root (b); elongated lateral root (c); flower (d); mature plants (e). f, Subcellular localization of AtCXE15. Images are confocal micrographs of lateral root, lateral root meristem, and lateral root epidermal cells (from left to right) in the transgenic *Arabidopsis* seedlings carrying a *pAtCXE15*:*AtCXE15*:*GFP* construct. The fluorescence from GFP is shown in green and from FM4-64 in red. Three independent transgenic lines were characterized for each genotype and representative seedlings were photographed. The experiments were repeated at least two times independently with similar results.

Extended Data Fig. 5| Hydrolytic activity of AtCXEs and AtD14 toward YLG and 4-nitrophenol acetate (4-NPA). a, Binding affinity of AtCXE15 with canonical SL (±)-5DS and non-canonical SL analogue (±)-MP3 assayed by microscale thermophoresis. Data points indicate the change in normalized fluorescence (Δ FNorm [‰]), and curves indicate the calculated fits. Mean

values of binding affinity (Kd) are shown, and error bars represent s.e. (n = 5-7 independent measurements). **b**, Hydrolytic kinetics of AtCXE15, AtD14, AtCXE10/GID1a, and AtCXE18 toward YLG. The 0.02 μM GST-tagged proteins were incubated with 1μM YLG to ensure better visualization of initial burst phase, and the enzymatic activity was defined by the change in fluorescein over 38 mins. The His-tagged AtCXE15 were also used to exclude potential effect of GST-tag on the enzymatic activity. Data are means ± s.d.; n = 6 technical replicates. **c**, Hydrolysis of YLG by AtCXE15 and AtD14 is attenuated by (±)-GR24 in a dose-dependent manner. Data are shown as means ± s.d.; n = 6 technical replicates. **d**, Hydrolytic kinetics of AtCXE15, AtD14, AtCXE10/GID1a, and AtCXE18 toward 4-NPA. 1 μM GST-tagged proteins were incubated with 100 μM 4-NPA for 30 min at 37 °C. The released 4-nitrophenol was monitored (Abs 405 nm). Data are shown as means ± s.d.; n = 3 independent replicates.

Extended Data Fig. 6| Characterization of the Moss CXEs and AtCXE5 orthologues from seed plants. a, Phylogeny of the putative CXE15 orthologues from seed plants, AtD14, and PpCXEs. Eight PpCXEs from *Physcomitrium patens* are collected using the AtCXE15 protein sequence as a query to search against Ensembl Plants database by Hmmer with default settings. Numbers are percent bootstrap values for 1,000 replicates. **b**,

Hydrolytic activities of PpCXE2, PpCXE5, PpCXE6, and PpCXE8 toward YLG. AtD14 was used as a positive control. Data are means ± s.d.; n = 6 technical replicates. **c**, Transcriptional response of *OsCXE17* and *BnaCXE15* to (±)-GR24. Transcript abundance of *CXE15* orthologues was monitored in 11-day-old seedlings after treatment with 5 μM (±)-GR24 for 3 h. Data were normalized to mock and shown as means ± s.d.; n = 3 biological replicates; two-tailed Student's *t*-test. **d**, The primary rosette branch number (upper panel) and relative transcript level of *AtCXE15* orthologues (bottom panel) in the transgenic *Arabidopsis* plants indicated. Three independent transgenic lines were characterized for each genotype. The means of branch number are shown as black lines. n = 3 biological replicates of at least 15 plants for each line. The qRT-PCR data are shown as means ± s.d.; n = 3 biological replicates from 20 seedlings for each line. The statistical analysis was performed by comparing that of Col-0 with each *CXE15*-*OE* genotype. *F* (degree of freedom) values are shown; The letters in **d** indicate statistical differences between genotypes determined by one-way ANOVA followed by Tukey's HSD test for multiple comparisons ($P<0.05$).

Extended Data Fig. 7| Transcriptional responses of *AtCXE15*, *AtMAX3*, *AtD14*, and *AtMAX2* to biotic and abiotic stimuli. Log_2-transformed relative

801 expression values of *AtCXE15*, *AtMAX3*, *AtD14* and *AtMAX2* in publicly
802 available microarray and RNA-seq data on biotic and abiotic stress treatments
803 (Genevestigator). NASC Arrays: flg22 (Seedling) (E-NASC-76). Gene
804 Expression Omnibus: 10 μM ABA (GSE28800); 50 μM ABA (GSE65016); 5h
805 sucrose (GSE37408); 2h ozone (GSE61542); flg22 and HrpZ (Leaf disc)
806 (GSE5615); salt stress (GSE46205); cold stress (GSE55835). ArrayExpress:
807 drought stress (E-MEXP-3713); 4h glucose (E-MEXP-475). Magenta, green
808 and white indicate upregulation, downregulation, and no change versus control
809 experiments, respectively.
810

References

1 Gomez-Roldan, V. *et al.* Strigolactone inhibition of shoot branching. *Nature* **455**, 189-194 (2008).

2 Akiyama, K., Matsuzaki, K. & Hayashi, H. Plant sesquiterpenes induce hyphal branching in arbuscular mycorrhizal fungi. *Nature* **435**, 824-827 (2005).

3 Tsuchiya, Y. *et al.* Probing strigolactone receptors in *Striga hermonthica* with fluorescence. *Science* **349**, 864-868 (2015).

4 Cook, C. E., Whichard, L. P., Turner, B., Wall, M. E. & Egley, G. H. Germination of witchweed (*Striga lutea Lour.*): isolation and properties of a potent stimulant. *Science* **154**, 1189-1190 (1966).

5 Umehara, M. *et al.* Inhibition of shoot branching by new terpenoid plant hormones. *Nature* **455**, 195-200 (2008).

6 Hamiaux, C. *et al.* DAD2 is an α/β hydrolase likely to be involved in the perception of the plant branching hormone, strigolactone. *Curr. Biol.* **22**, 2032-2036 (2012).

7 Yoneyama, K. *et al.* Which are the major players, canonical or non-canonical strigolactones? *J. Exp. Bot.* **69**, 2231-2239 (2018).

8 Yao, R. *et al.* DWARF14 is a non-canonical hormone receptor for strigolactone. *Nature* **536**, 469-473 (2016).

9 Chevalier, F. *et al.* Strigolactone promotes degradation of DWARF14, an α/β hydrolase essential for strigolactone signaling in *Arabidopsis*. *Plant Cell* **26**, 1134-1150 (2014).

10 Zhao, L. *et al.* Crystal structures of two phytohormone signal-transducing α/β hydrolases: karrikin-signaling KAI2 and strigolactone-signaling DWARF14. *Cell Res.* **23**, 436-439 (2013).

11 Zhao, L. *et al.* Destabilization of strigolactone receptor DWARF14 by binding of ligand and E3-ligase signaling effector DWARF3. *Cell Res.* **25**, 1219-1236 (2015).

12 Seto, Y. *et al.* Strigolactone perception and deactivation by a hydrolase receptor DWARF14. *Nat. Commun.* **10**, 1-10 (2019).

13 Zhou, F. *et al.* D14–SCF D3-dependent degradation of D53 regulates strigolactone signalling. *Nature* **504**, 406-410 (2013).

14 Wang, L. *et al.* Transcriptional regulation of strigolactone signalling in *Arabidopsis*. *Nature* **583**, 277-281 (2020).

15 Shabek, N. *et al.* Structural plasticity of D3–D14 ubiquitin ligase in strigolactone signalling. *Nature* **563**, 652-656 (2018).

16 Wang, L. *et al.* Strigolactone signaling in *Arabidopsis* regulates shoot development by targeting D53-like SMXL repressor proteins for ubiquitination and degradation. *Plant Cell* **27**, 3128-3142 (2015).

17 Nelson, D. C. *et al.* F-box protein MAX2 has dual roles in karrikin and strigolactone signaling in *Arabidopsis thaliana*. *Proc. Natl Acad. Sci. USA* **108**, 8897-8902 (2011).

18 Qu, B., Qin, Y. & Bai, Y. From signaling to function: how strigolactones regulate plant development. *Sci. China Life Sci.* **63**, 1768-1770 (2020).

19 Liang, Y., Ward, S., Li, P., Bennett, T. & Leyser, O. SMAX1-LIKE7 signals from the nucleus to regulate shoot development in *Arabidopsis* via partially EAR motif-independent mechanisms. *Plant Cell* **28**, 1581-1601 (2016).

20 Dun, E. A., de Saint Germain, A., Rameau, C. & Beveridge, C. A. Dynamics of strigolactone function and shoot branching responses in *Pisum sativum*. *Mol. Plant* **6**, 128-140 (2013).

21 Braun, N. *et al.* The pea TCP transcription factor PsBRC1 acts downstream of strigolactones to control shoot branching. *Plant Physiol.* **158**, 225-238 (2012).

22 Shen, J. *et al.* CsBRC1 inhibits axillary bud outgrowth by directly repressing the auxin efflux carrier CsPIN3 in cucumber. *Proc. Natl. Acad. Sci. USA* **116**, 17105-17114 (2019).

23 Martín-Trillo, M. *et al.* Role of tomato *BRANCHED1-like* genes in the control of shoot branching. *Plant J.* **67**, 701-714 (2011).

24 de Saint Germain, A. *et al.* An histidine covalent receptor and butenolide complex mediates strigolactone perception. *Nat. Chem. Biol.* **12**, 787-794 (2016).

25 Soundappan, I. *et al.* SMAX1-LIKE/D53 family members enable distinct MAX2-dependent responses to strigolactones and karrikins in *Arabidopsis*. *Plant Cell* **27**, 3143-3159 (2015).

26 Xu, K. *et al.* A genome-wide transcriptome profiling reveals the early molecular events during callus initiation in *Arabidopsis* multiple organs. *Genomics* **100**, 116-124 (2012).

27 Wang, B., Smith, S. M. & Li, J. Genetic regulation of shoot architecture. *Annu. Rev. Plant Biol.* **69**, 437-468 (2018).

28 Marshall, S. D., Putterill, J. J., Plummer, K. M. & Newcomb, R. D. The carboxylesterase gene family from *Arabidopsis thaliana*. *J. Mol. Evol.* **57**, 487-500 (2003).

29 Murase, K., Hirano, Y., Sun, T.-p. & Hakoshima, T. Gibberellin-induced DELLA recognition by the gibberellin receptor GID1. *Nature* **456**, 459-463 (2008).

30 Yoshida, H. *et al.* Evolution and diversification of the plant gibberellin receptor GID1. *Proc. Natl Acad. Sci. USA* **115**, E7844-E7853 (2018).

31 Hayward, A., Stirnberg, P., Beveridge, C. & Leyser, O. Interactions between auxin and strigolactone in shoot branching control. *Plant Physiol.* **151**, 400-412 (2009).

32 Foo, E. *et al.* The branching gene *RAMOSUS1* mediates interactions among two novel signals and auxin in pea. *Plant Cell* **17**, 464-474 (2005).

33 Johnson, X. *et al.* Branching genes are conserved across species. Genes controlling a novel signal in pea are coregulated by other long-distance signals. *Plant Physiol.* **142**, 1014-1026 (2006).

34 Snowden, K. C. *et al.* The *Decreased apical dominance1*/*Petunia hybrida CAROTENOID CLEAVAGE DIOXYGENASE8* gene affects branch production and plays a role in leaf senescence, root growth, and flower development. *Plant Cell* **17**, 746-759 (2005).

35 Arite, T. *et al.* DWARF10, an RMS1/MAX4/DAD1 ortholog, controls lateral bud outgrowth in rice. *Plant J.* **51**, 1019-1029 (2007).

36 Simons, J. L., Napoli, C. A., Janssen, B. J., Plummer, K. M. & Snowden, K. C. Analysis of the *DECREASED APICAL DOMINANCE* genes of *petunia* in the control of axillary branching. *Plant Physiol.* **143**, 697-706 (2007).

37 Alder, A. *et al.* The path from β-carotene to carlactone, a strigolactone-like plant hormone. *Science* **335**, 1348-1351 (2012).

38 Jamil, M. *et al.* Methyl phenlactonoates are efficient strigolactone analogs with simple structure. *J. Exp. Bot.* **69**, 2319-2331 (2018).

39 Beveridge, C. A., Ross, J. J. & Murfet, I. C. Branching in Pea: action of genes *Rms3* and *Rms4*. *Plant Physiol.* **110**, 859-865 (1996).

40 Beveridge, C. A., Ross, J. J. & Murfet, I. C. Branching mutant *rms-2* in *Pisum sativum*: grafting studies and endogenous indole-3-acetic acid levels. *Plant Physiol.* **104**, 953-959 (1994).

41 Tsuchiya, Y. *et al.* A small-molecule screen identifies new functions for the plant hormone strigolactone. *Nat. Chem. Biol.* **6**, 741-749 (2010).

42 Jia, K., Luo, Q., He, S., Lu, X. & Yang, H. Strigolactone-regulated hypocotyl elongation is dependent on cryptochrome and phytochrome signaling pathways in *Arabidopsis*. *Mol. Plant* **7**, 528-540 (2014).

43 Guo, Y., Zheng, Z., La Clair, J. J., Chory, J. & Noel, J. P. Smoke-derived karrikin perception by the α/β-hydrolase KAI2 from *Arabidopsis*. *Proc. Natl. Acad. Sci. USA* **110**, 8284-8289 (2013).

44 Conn, C. E. & Nelson, D. C. Evidence that KARRIKIN-INSENSITIVE2 (KAI2) receptors may perceive an unknown signal that is not karrikin or strigolactone. *Front. Plant Sci.* **6**, 1219 (2015).

45 Sorefan, K. *et al.* MAX4 and RMS1 are orthologous dioxygenase-like genes that regulate shoot branching in *Arabidopsis* and pea. *Genes Dev.* **17**, 1469-1474 (2003).

46 Booker, J. *et al. MAX1* encodes a cytochrome P450 family member that acts downstream of *MAX3*/*4* to produce a carotenoid-derived branch-inhibiting hormone. *Dev. Cell* **8**, 443-449 (2005).

47 Booker, J. *et al.* MAX3/CCD7 is a carotenoid cleavage dioxygenase required for the synthesis of a novel plant signaling molecule. *Curr. Biol.* **14**, 1232-1238 (2004).

48 Abe, S. *et al.* Carlactone is converted to carlactonoic acid by MAX1 in *Arabidopsis* and its methyl ester can directly interact with AtD14 *in vitro*. *Proc. Natl Acad. Sci. USA* **111**, 18084-18089 (2014).

49 Cummins, I., Landrum, M., Steel, P. G. & Edwards, R. Structure activity studies with xenobiotic substrates using carboxylesterases isolated from *Arabidopsis thaliana*. *Phytochemistry* **68**, 811-818 (2007).

50 Nakajima, M. *et al.* Identification and characterization of *Arabidopsis* gibberellin receptors. *Plant J.* **46**, 880-889 (2006).

51 Xie, X. Structural diversity of strigolactones and their distribution in the plant kingdom. *J. Pestic. Sci.*, J16-02 (2016).

52 Chesterfield, R. J., Vickers, C. E. & Beveridge, C. A. Translation of strigolactones from plant hormone to agriculture: achievements, future perspectives, and challenges. *Trends Plant Sci.* **25**, 1087-1106 (2020).

53 Woo, S. & McErlean, C. S. P. Total synthesis and stereochemical confirmation of heliolactone. *Org. Lett.* **21**, 4215-4218 (2019).

54 Dieckmann, M. C., Dakas, P. Y. & De Mesmaeker, A. Synthetic access to noncanonical strigolactones: syntheses of carlactonic acid and methyl carlactonoate. *J. Org. Chem.* **83**, 125-135 (2018).

55 Yoneyama, K. *et al.* Hydroxyl carlactone derivatives are predominant strigolactones in *Arabidopsis*. *Plant Direct* **4**, e00219 (2020).

56 Brewer, P. B. *et al.* LATERAL BRANCHING OXIDOREDUCTASE acts in the final stages of strigolactone biosynthesis in *Arabidopsis*. *Proc. Natl. Acad. Sci. USA* **113**, 6301-6306 (2016).

57 Nomura, T., Murase, T., Ogita, S. & Kato, Y. Molecular identification of tuliposide B-converting enzyme: a lactone-forming carboxylesterase from the pollen of tulip. *Plant J.* **83**, 252-262 (2015).

58 Walker, C. H., Siu-Ting, K., Taylor, A., O'Connell, M. J. & Bennett, T. Strigolactone synthesis is ancestral in land plants, but canonical strigolactone signalling is a flowering plant innovation. *BMC Biol.* **17**, 70 (2019).

59 Lopez-Obando, M. *et al.* Structural modelling and transcriptional responses highlight a clade of PpKAI2-LIKE genes as candidate receptors for strigolactones in *Physcomitrella patens*. *Planta* **243**, 1441-1453 (2016).

60 Bürger, M. *et al.* Structural basis of karrikin and non-natural strigolactone perception in *Physcomitrella patens*. *Cell Rep.* **26**, 855-865 (2019).

61 Wakabayashi, T. *et al.* Direct conversion of carlactonoic acid to orobanchol by cytochrome P450 CYP722C in strigolactone biosynthesis. *Sci. Adv.* **5**, eaax9067 (2019).

62 Zheng, M. *et al.* Knockout of two *BnaMAX1* homologs by CRISPR/Cas9-targeted mutagenesis improves plant architecture and increases yield in rapeseed (*Brassica napus* L.). *Plant Biotechnol. J.* **18**, 644-654 (2020).

63 Kalliola, M. *et al.* Differential role of MAX2 and strigolactones in pathogen, ozone, and stomatal responses. *Plant Direct* **4**, e00206 (2020).

64 Van Ha, C. *et al.* Positive regulatory role of strigolactone in plant responses to drought and salt stress. *Proc. Natl Acad. Sci. USA* **111**, 851-856 (2014).

65 Cooper, J. W. *et al.* Strigolactones positively regulate chilling tolerance in pea and in *Arabidopsis*. *Plant Cell Environ.* **41**, 1298-1310 (2018).

66 Bu, Q. *et al.* Regulation of drought tolerance by the F-box protein MAX2 in *Arabidopsis*. *Plant Physiol.* **164**, 424-439 (2014).

67 Gershater, M. C. & Edwards, R. Regulating biological activity in plants with carboxylesterases. *Plant Sci.* **173**, 579-588 (2007).

68 Proust, H. *et al.* Strigolactones regulate protonema branching and act as a quorum sensing-like signal in the moss *Physcomitrella patens*. *Development* **138**, 1531-1539 (2011).

69 Waters, M. T. *et al.* Specialisation within the DWARF14 protein family confers distinct responses to karrikins and strigolactones in *Arabidopsis*. *Development* **139**, 1285-1295 (2012).

70 Stirnberg, P., van De Sande, K. & Leyser, H. M. MAX1 and MAX2 control shoot lateral branching in *Arabidopsis. Development* **129**, 1131-1141 (2002).

71 Mangnus, E. M., Van Vliet, L. A., Vandenput, D. A. L. & Zwanenburg, B. Structural modifications of strigol analogs. Influence of the B and C rings on the bioactivity of the germination stimulant GR24. *J. Agric. Food Chem.* **40**, 1222-1229 (1992).

72 Xing, H. *et al.* A CRISPR/Cas9 toolkit for multiplex genome editing in plants. *BMC Plant Bio.* **14**, 327 (2014).

73 One Thousand Plant Transcriptomes Initiative. One thousand plant transcriptomes and the phylogenomics of green plants. *Nature* **574**, 679 (2019).

74 Ni, M. *et al.* Strength and tissue specificity of chimeric promoters derived from the octopine and mannopine synthase genes. *Plant J.* **7**, 661-676 (1995).

75 Hu, Y., Xie, Q. & Chua, N.-H. The *Arabidopsis* auxin-inducible gene ARGOS controls lateral organ size. *Plant Cell* **15**, 1951-1961 (2003).

76 Clough, S. J. & Bent, A. F. Floral dip: a simplified method for *Agrobacterium*-mediated transformation of *Arabidopsis thaliana*. *Plant J.* **16**, 735-743 (1998).

77 Xu, E., Vaahtera, L. & Brosché, M. Roles of defense hormones in the regulation of ozone-induced changes in gene expression and cell death. *Mol. Plant* **8**, 1776-1794 (2015).

78 Cui, D. *et al.* The *Arabidopsis* IDD14, IDD15, and IDD16 cooperatively regulate lateral organ morphogenesis and gravitropism by promoting auxin biosynthesis and transport. *PLoS Genet.* **9**, e1003759 (2013).

79 Melnyk, C. W. Grafting with *Arabidopsis thaliana*. *Methods Mol. Biol.* **1497**, 9-18 (2017).

80 Liu, C. *et al.* Two *Arabidopsis* receptor-like cytoplasmic kinases SZE1 and SZE2 associate with the ZAR1-ZED1 complex and are required for effector-triggered immunity. *Mol. Plant* **12**, 967-983 (2019).

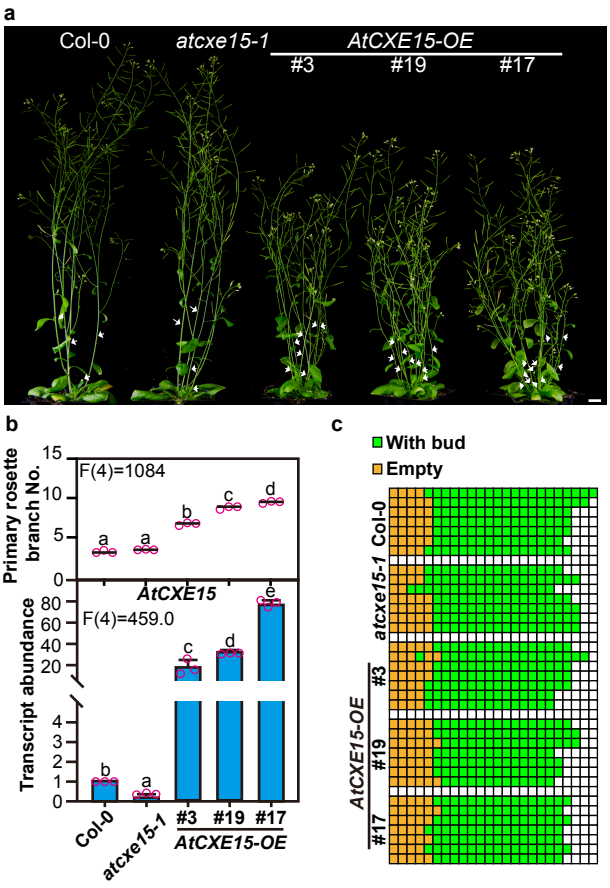
a
Col-0
atcxe15-1
AtCXE15-OE
#3
#19
#17
b
Primary rosette branch No.
F(4)=1084
AtCXE15
F(4)=459.0
Transcript abundance
Col-0
atcxe15-1
#3
#19
#17
AtCXE15-OE
c
With bud
Empty
Col-0
atcxe15-1
AtCXE15-OE
#3
#19
#17

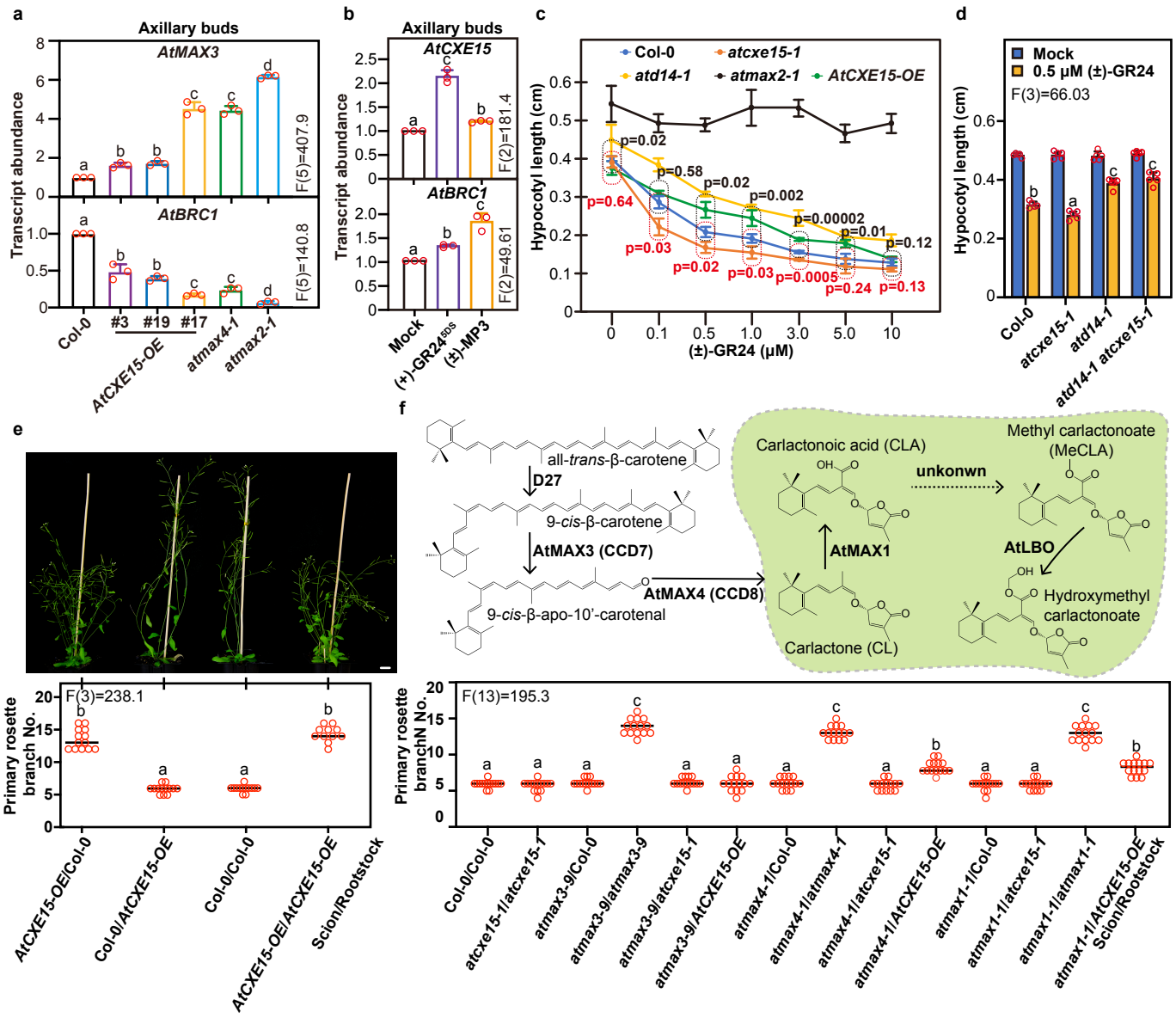
a
Axillary buds
AtMAX3
AtBRC1
Transcript abundance
F(5)=407.9
F(5)=140.8
Col-0
#3
#19
#17
AtCXE15-OE
atmax4-1
atmax2-1
b
Axillary buds
AtCXE15
AtBRC1
F(2)=181.4
F(2)=49.61
Mock
(+)-GR24 5DS
(±)-MP3
c
Col-0
atcxe15-1
atd14-1
atmax2-1
AtCXE15-OE
Hypocotyl length (cm)
p=0.64
p=0.02
p=0.58
p=0.02
p=0.002
p=0.00002
p=0.01
p=0.12
p=0.03
p=0.02
p=0.03
p=0.0005
p=0.24
p=0.13
(±)-GR24 (μM)
d
Mock
0.5 μM (±)-GR24
F(3)=66.03
Hypocotyl length (cm)
Col-0
atcxe15-1
atd14-1
atd14-1 atcxe15-1
e
f
all-trans-β-carotene
D27
9-cis-β-carotene
AtMAX3 (CCD7)
9-cis-β-apo-10'-carotenal
AtMAX4 (CCD8)
Carlactonoic acid (CLA)
unkonwn
Methyl carlactonoate (MeCLA)
AtMAX1
AtLBO
Hydroxymethyl carlactonoate
Carlactone (CL)
F(3)=238.1
Primary rosette branch No.
AtCXE15-OE/Col-0
Col-0/AtCXE15-OE
Col-0/Col-0
AtCXE15-OE/AtCXE15-OE
Scion/Rootstock
F(13)=195.3
Primary rosette branchN No.
Col-0/Col-0
atcxe15-1/atcxe15-1
atmax3-9/Col-0
atmax3-9/atmax3-9
atmax3-9/atcxe15-1
atmax3-9/AtCXE15-OE
atmax4-1/Col-0
atmax4-1/atmax4-1
atmax4-1/atcxe15-1
atmax4-1/AtCXE15-OE
atmax1-1/Col-0
atmax1-1/atcxe15-1
atmax1-1/atmax1-1
atmax1-1/AtCXE15-OE
Scion/Rootstock

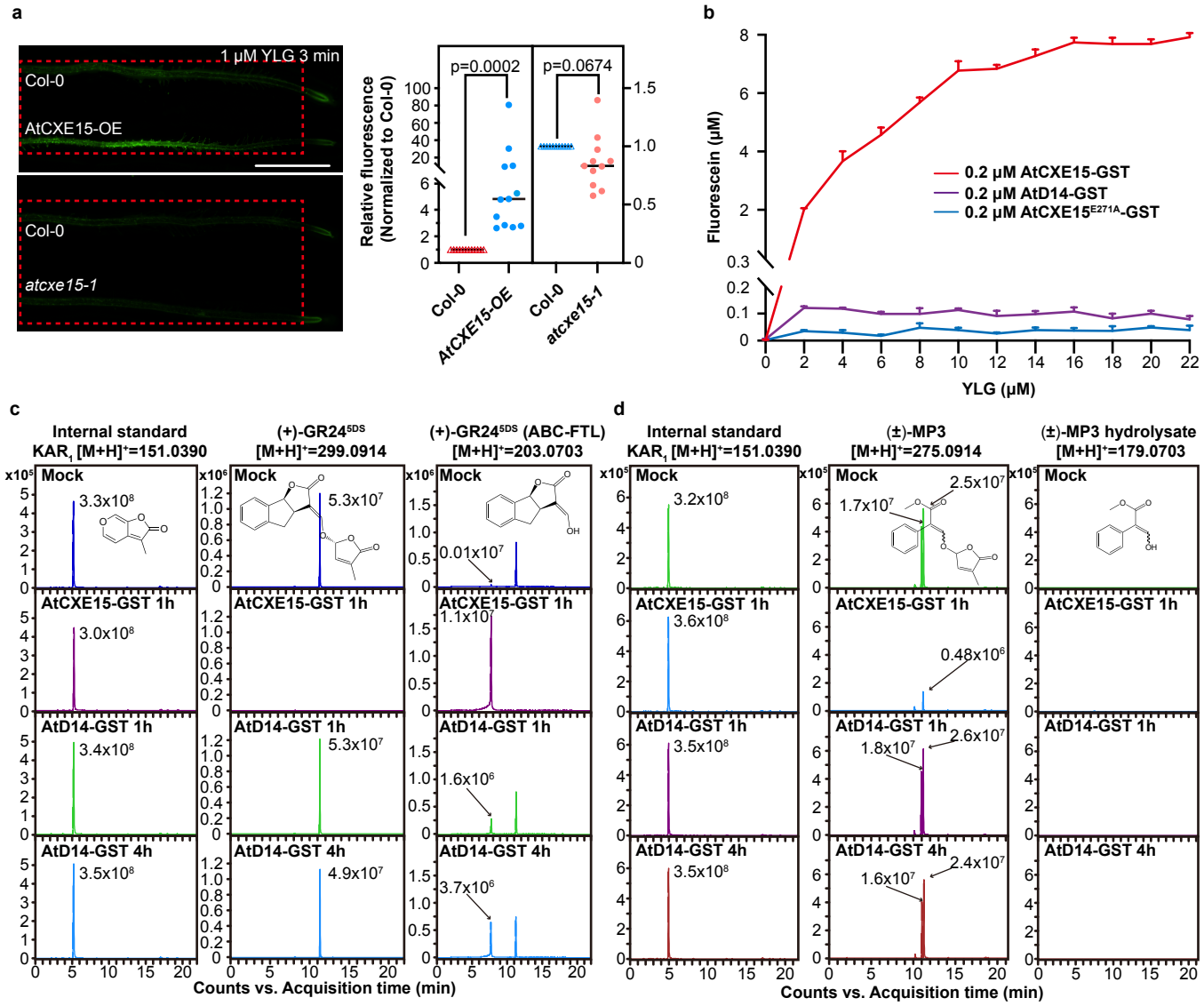
a
1 μM YLG 3 min
Col-0
AtCXE15-OE
Col-0
atcxe15-1
Relative fluorescence (Normalized to Col-0)
p=0.0002
p=0.0674
Col-0
AtCXE15-OE
Col-0
atcxe15-1
b
Fluorescein (μM)
0.2 μM AtCXE15-GST
0.2 μM AtD14-GST
0.2 μM AtCXE15E271A-GST
YLG (μM)
c
Internal standard
KAR1 [M+H]+=151.0390
(+)-GR245DS
[M+H]+=299.0914
(+)-GR245DS (ABC-FTL)
[M+H]+=203.0703
Mock
AtCXE15-GST 1h
AtD14-GST 1h
AtD14-GST 4h
3.3x10^8
5.3x10^7
0.01x10^7
3.0x10^8
1.1x10^7
3.4x10^8
5.3x10^7
1.6x10^6
3.5x10^8
4.9x10^7
3.7x10^6
Counts vs. Acquisition time (min)
d
Internal standard
KAR1 [M+H]+=151.0390
(±)-MP3
[M+H]+=275.0914
(±)-MP3 hydrolysate
[M+H]+=179.0703
Mock
AtCXE15-GST 1h
AtD14-GST 1h
AtD14-GST 4h
3.2x10^8
2.5x10^7
1.7x10^7
3.6x10^8
0.48x10^6
3.5x10^8
2.6x10^7
1.8x10^7
3.5x10^8
2.4x10^7
1.6x10^7
Counts vs. Acquisition time (min)

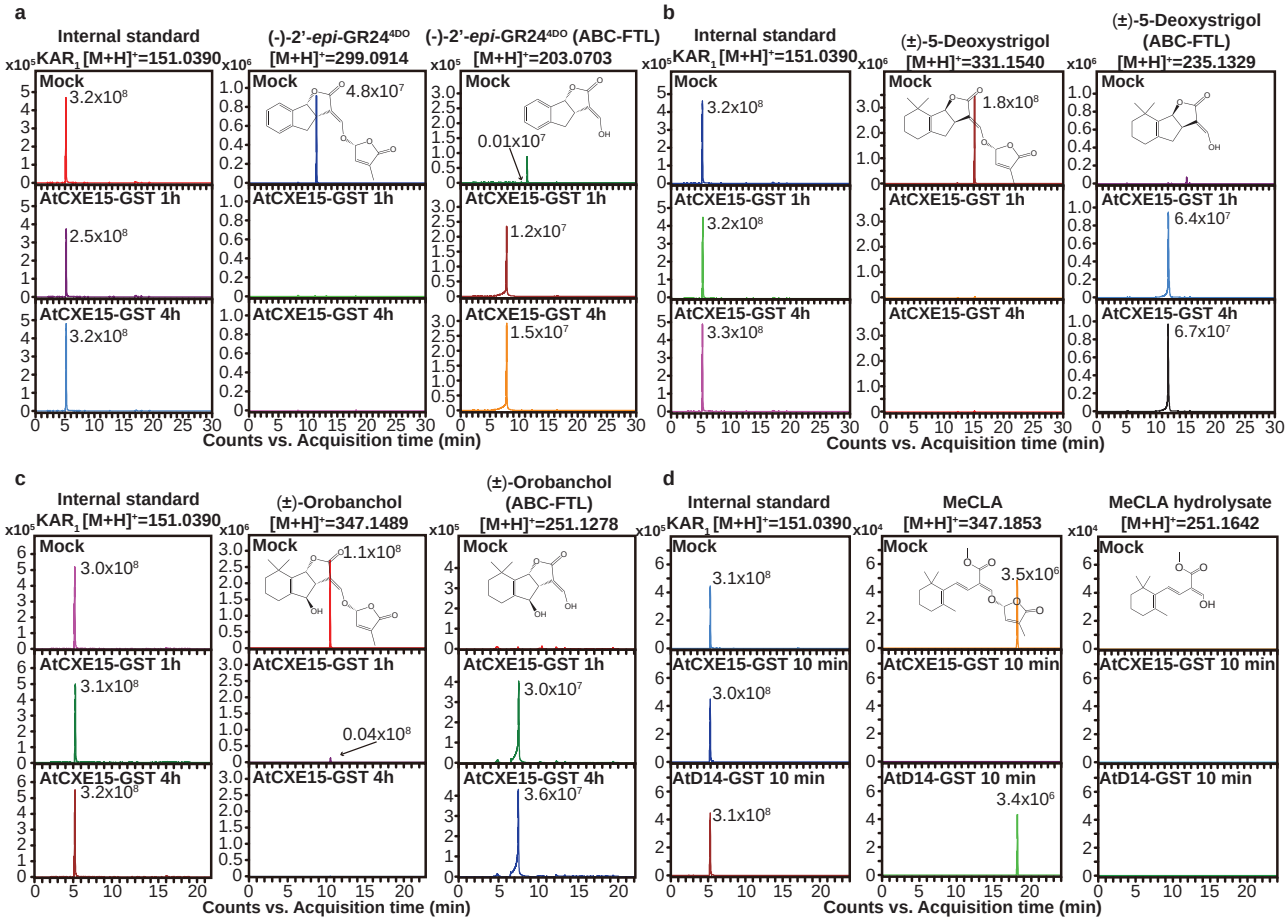
a
Internal standard
KAR1 [M+H]+=151.0390
(-)-2'-epi-GR24 4DO
[M+H]+=299.0914
(-)-2'-epi-GR24 4DO (ABC-FTL)
[M+H]+=203.0703
Mock
3.2x10^8
4.8x10^7
0.01x10^7
AtCXE15-GST 1h
2.5x10^8
1.2x10^7
AtCXE15-GST 4h
3.2x10^8
1.5x10^7
b
Internal standard
KAR1 [M+H]+=151.0390
(±)-5-Deoxystrigol
[M+H]+=331.1540
(±)-5-Deoxystrigol
(ABC-FTL)
[M+H]+=235.1329
3.2x10^8
1.8x10^8
6.4x10^7
3.2x10^8
3.3x10^8
6.7x10^7
Counts vs. Acquisition time (min)
c
Internal standard
KAR1 [M+H]+=151.0390
(±)-Orobanchol
[M+H]+=347.1489
(±)-Orobanchol
(ABC-FTL)
[M+H]+=251.1278
3.0x10^8
1.1x10^8
3.1x10^8
0.04x10^8
3.2x10^8
3.0x10^7
3.6x10^7
d
Internal standard
KAR1 [M+H]+=151.0390
MeCLA
[M+H]+=347.1853
MeCLA hydrolysate
[M+H]+=251.1642
AtCXE15-GST 10 min
AtD14-GST 10 min
3.1x10^8
3.5x10^6
3.0x10^8
3.1x10^8
3.4x10^6
Counts vs. Acquisition time (min)

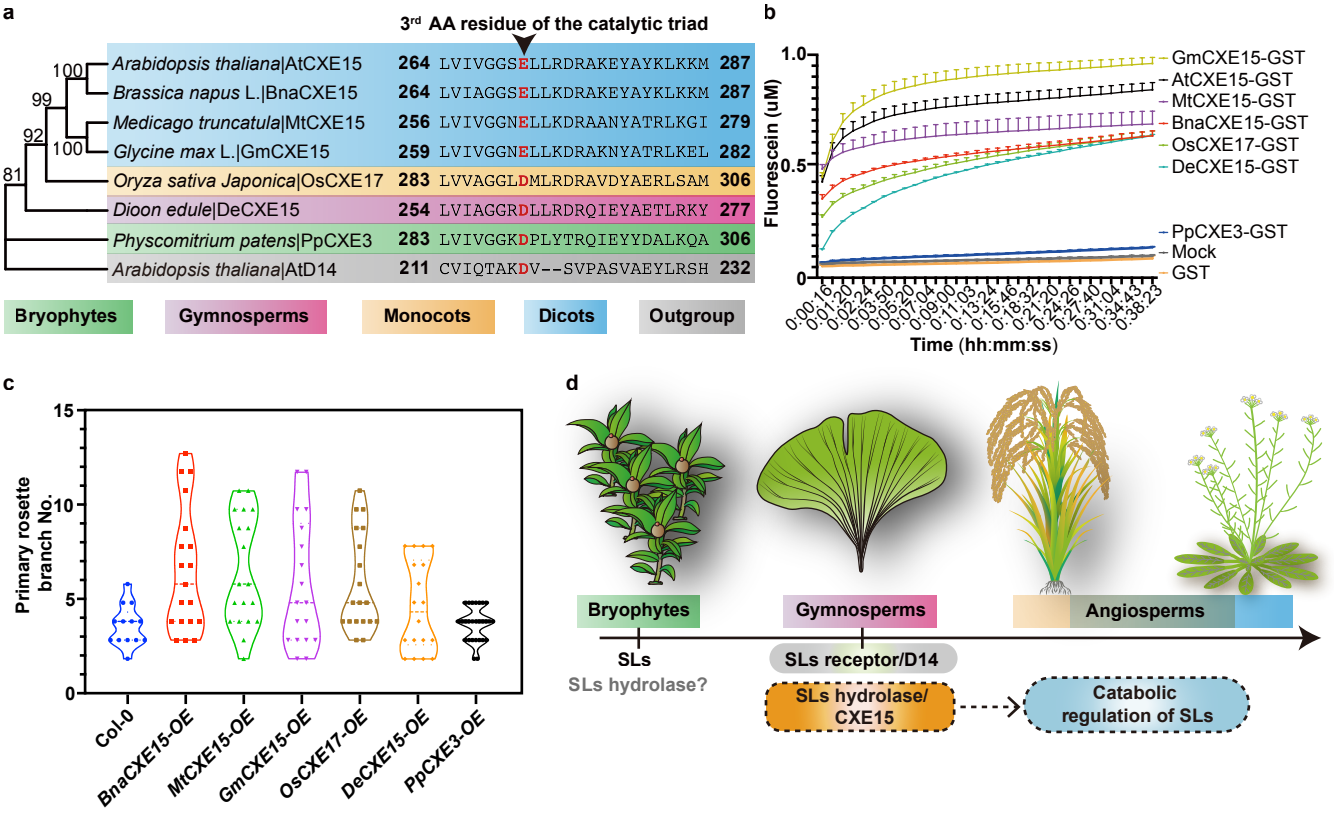
a
3rd AA residue of the catalytic triad
Arabidopsis thaliana|AtCXE15 264 LVIVGGSELLRDRAKEYAYKLKKM 287
Brassica napus L.|BnaCXE15 264 LVIAGGSELLKDRAKEYAYKLKKM 287
Medicago truncatula|MtCXE15 256 LVIVGGNELLKDRAANYATRLKGI 279
Glycine max L.|GmCXE15 259 LVIVGGNELLKDRAKNYATRLKEL 282
Oryza sativa Japonica|OsCXE17 283 LVVAGGLDMLRDRAVDYAERLSAM 306
Dioon edule|DeCXE15 254 LVIAGGRDLLRDRQIEYAETLRKY 277
Physcomitrium patens|PpCXE3 283 LVIVGGKDPLYTRQIEYYDALKQA 306
Arabidopsis thaliana|AtD14 211 CVIQTAKDV--SVPASVAEYLRSH 232
100
99
92
100
81
Bryophytes
Gymnosperms
Monocots
Dicots
Outgroup
b
Fluorescein (uM)
1.0
0.5
0
Time (hh:mm:ss)
GmCXE15-GST
AtCXE15-GST
MtCXE15-GST
BnaCXE15-GST
OsCXE17-GST
DeCXE15-GST
PpCXE3-GST
Mock
GST
c
Primary rosette branch No.
15
10
5
0
Col-0
BnaCXE15-OE
MtCXE15-OE
GmCXE15-OE
OsCXE17-OE
DeCXE15-OE
PpCXE3-OE
d
Bryophytes
Gymnosperms
Angiosperms
SLs
SLs hydrolase?
SLs receptor/D14
SLs hydrolase/ CXE15
Catabolic regulation of SLs

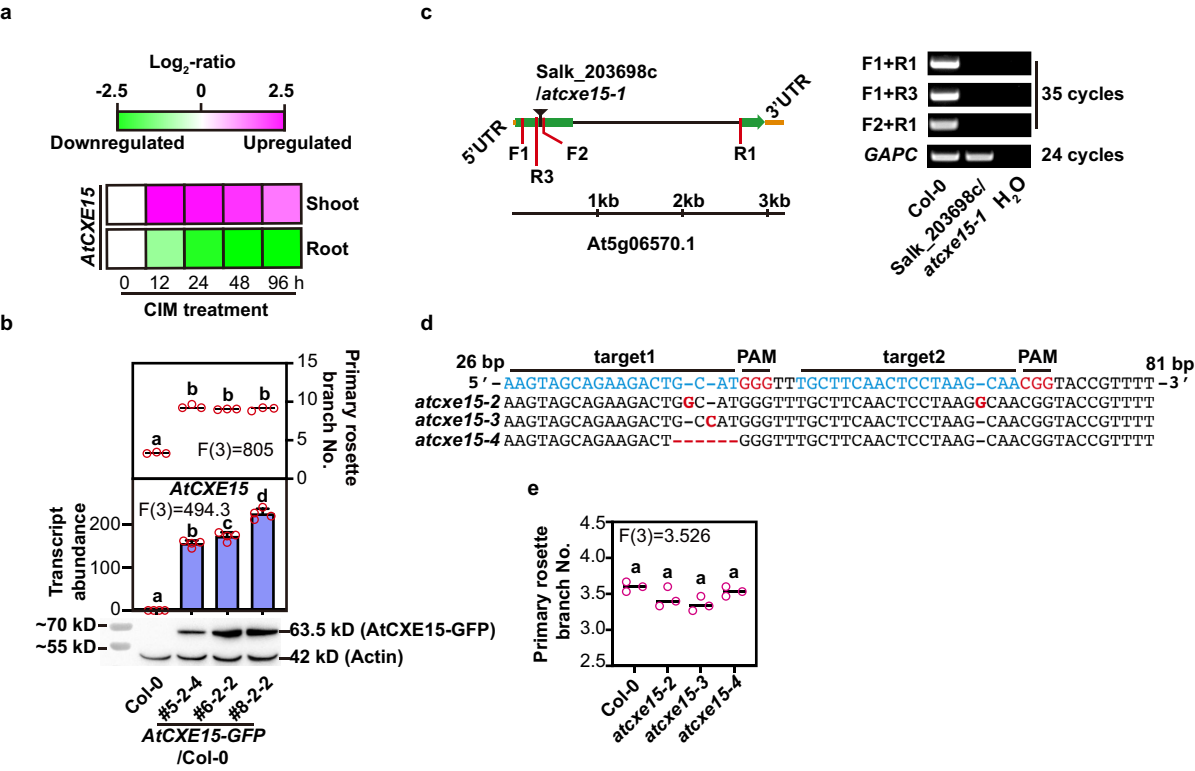
a
Log2-ratio
-2.5
0
2.5
Downregulated
Upregulated
AtCXE15
Shoot
Root
0 12 24 48 96 h
CIM treatment
b
Primary rosette branch No.
F(3)=805
AtCXE15
F(3)=494.3
Transcript abundance
~70 kD
~55 kD
63.5 kD (AtCXE15-GFP)
42 kD (Actin)
Col-0
#5-2-4
#6-2-2
#8-2-2
AtCXE15-GFP /Col-0
c
Salk_203698c /atcxe15-1
5'UTR
3'UTR
F1
F2
R1
R3
1kb
2kb
3kb
At5g06570.1
F1+R1
F1+R3
F2+R1
GAPC
35 cycles
24 cycles
Col-0
Salk_203698c/ atcxe15-1
H2O
d
26 bp
target1
PAM
target2
PAM
81 bp
5'-AAGTAGCAGAAGACTG-C-ATGGGTTTGCTTCAACTCCTAAG-CAACGGTACCGTTTT-3'
atcxe15-2 AAGTAGCAGAAGACTGGC-ATGGGTTTGCTTCAACTCCTAAGGCAACGGTACCGTTTT
atcxe15-3 AAGTAGCAGAAGACTG-CCATGGGTTTGCTTCAACTCCTAAG-CAACGGTACCGTTTT
atcxe15-4 AAGTAGCAGAAGACT------GGGTTTGCTTCAACTCCTAAG-CAACGGTACCGTTTT
e
Primary rosette branch No.
F(3)=3.526
Col-0
atcxe15-2
atcxe15-3
atcxe15-4

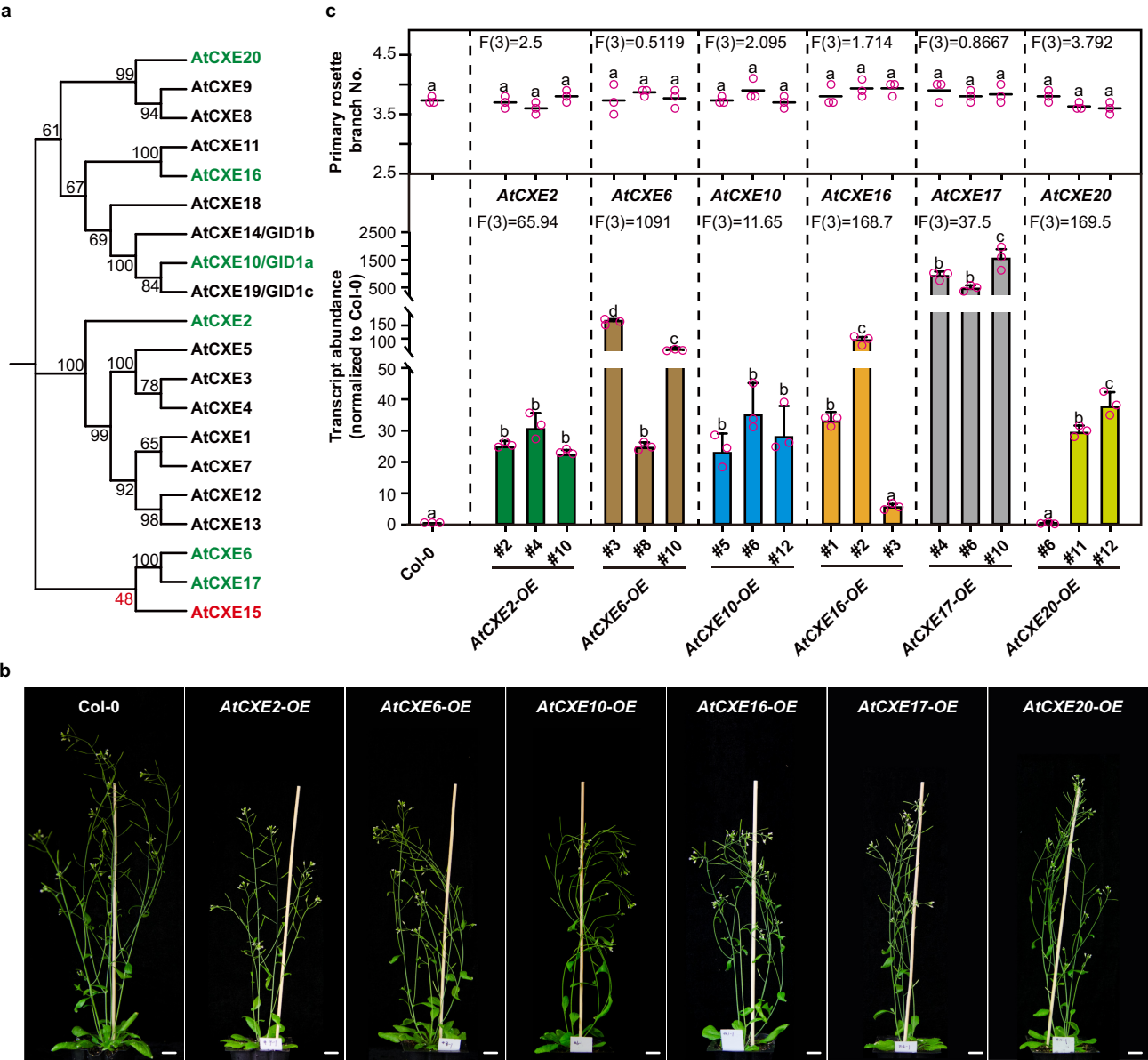
a
AtCXE20
AtCXE9
AtCXE8
AtCXE11
AtCXE16
AtCXE18
AtCXE14/GID1b
AtCXE10/GID1a
AtCXE19/GID1c
AtCXE2
AtCXE5
AtCXE3
AtCXE4
AtCXE1
AtCXE7
AtCXE12
AtCXE13
AtCXE6
AtCXE17
AtCXE15
99
94
61
100
67
69
100
84
100
100
78
99
65
92
98
100
48
c
Primary rosette branch No.
F(3)=2.5
F(3)=0.5119
F(3)=2.095
F(3)=1.714
F(3)=0.8667
F(3)=3.792
AtCXE2
AtCXE6
AtCXE10
AtCXE16
AtCXE17
AtCXE20
F(3)=65.94
F(3)=1091
F(3)=11.65
F(3)=168.7
F(3)=37.5
F(3)=169.5
Transcript abundance (normalized to Col-0)
Col-0
#2
#4
#10
#3
#8
#10
#5
#6
#12
#1
#2
#3
#4
#6
#10
#6
#11
#12
AtCXE2-OE
AtCXE6-OE
AtCXE10-OE
AtCXE16-OE
AtCXE17-OE
AtCXE20-OE
b
Col-0
AtCXE2-OE
AtCXE6-OE
AtCXE10-OE
AtCXE16-OE
AtCXE17-OE
AtCXE20-OE

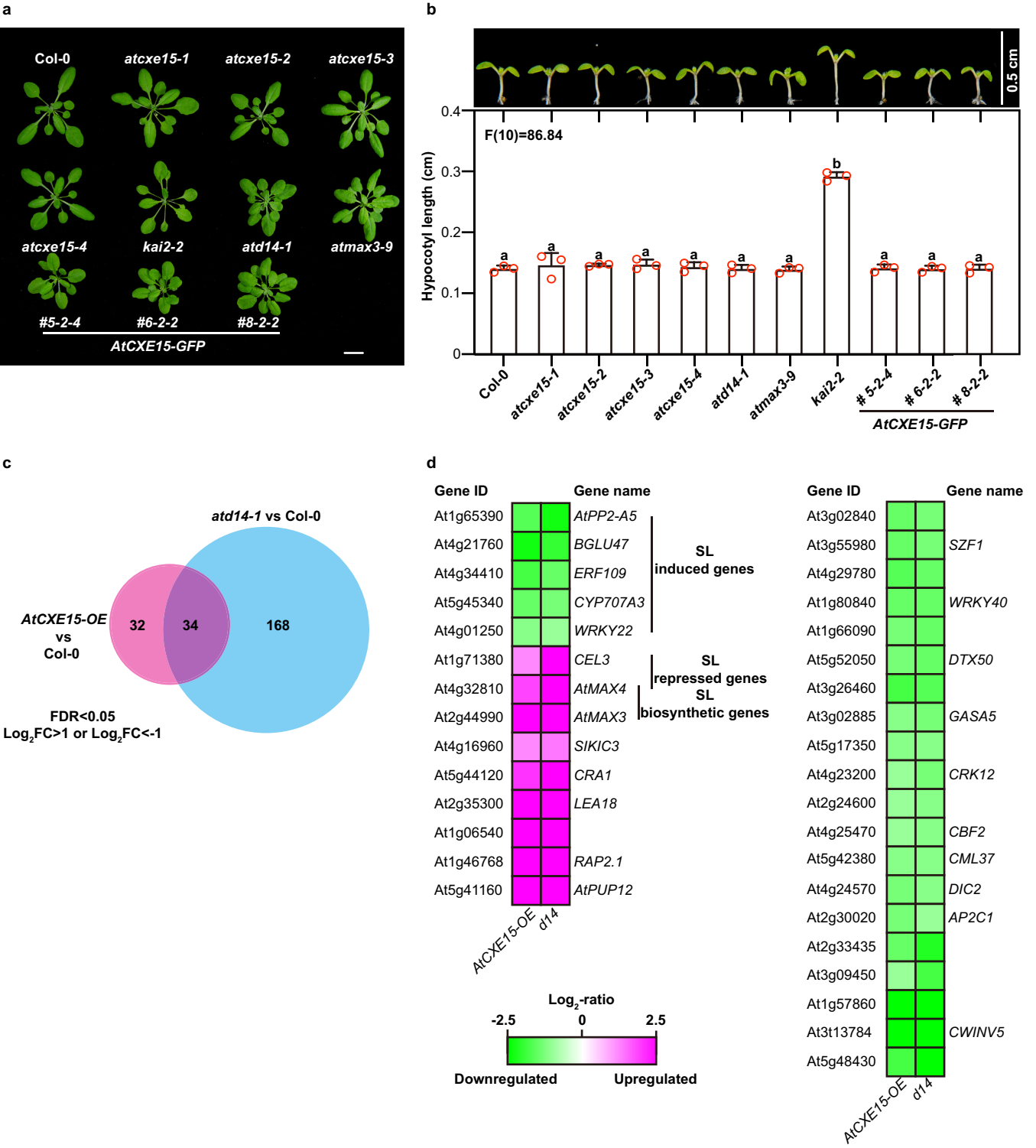
a
Col-0
atcxe15-1
atcxe15-2
atcxe15-3
atcxe15-4
kai2-2
atd14-1
atmax3-9
#5-2-4
#6-2-2
#8-2-2
AtCXE15-GFP
b
0.5 cm
F(10)=86.84
Hypocotyl length (cm)
0.4
0.3
0.2
0.1
0
a
b
Col-0
atcxe15-1
atcxe15-2
atcxe15-3
atcxe15-4
atd14-1
atmax3-9
kai2-2
5-2-4
6-2-2
8-2-2
AtCXE15-GFP
c
atd14-1 vs Col-0
AtCXE15-OE
vs
Col-0
32
34
168
FDR<0.05
Log2FC>1 or Log2FC<-1
d
Gene ID
Gene name
At1g65390
AtPP2-A5
At4g21760
BGLU47
At4g34410
ERF109
At5g45340
CYP707A3
At4g01250
WRKY22
SL
induced genes
At1g71380
CEL3
At4g32810
AtMAX4
At2g44990
AtMAX3
SL
repressed genes
SL
biosynthetic genes
At4g16960
SIKIC3
At5g44120
CRA1
At2g35300
LEA18
At1g06540
At1g46768
RAP2.1
At5g41160
AtPUP12
AtCXE15-OE
d14
Log2-ratio
-2.5
0
2.5
Downregulated
Upregulated
Gene ID
Gene name
At3g02840
At3g55980
SZF1
At4g29780
At1g80840
WRKY40
At1g66090
At5g52050
DTX50
At3g26460
At3g02885
GASA5
At5g17350
At4g23200
CRK12
At2g24600
At4g25470
CBF2
At5g42380
CML37
At4g24570
DIC2
At2g30020
AP2C1
At2g33435
At3g09450
At1g57860
At3t13784
CWINV5
At5g48430
AtCXE15-OE
d14

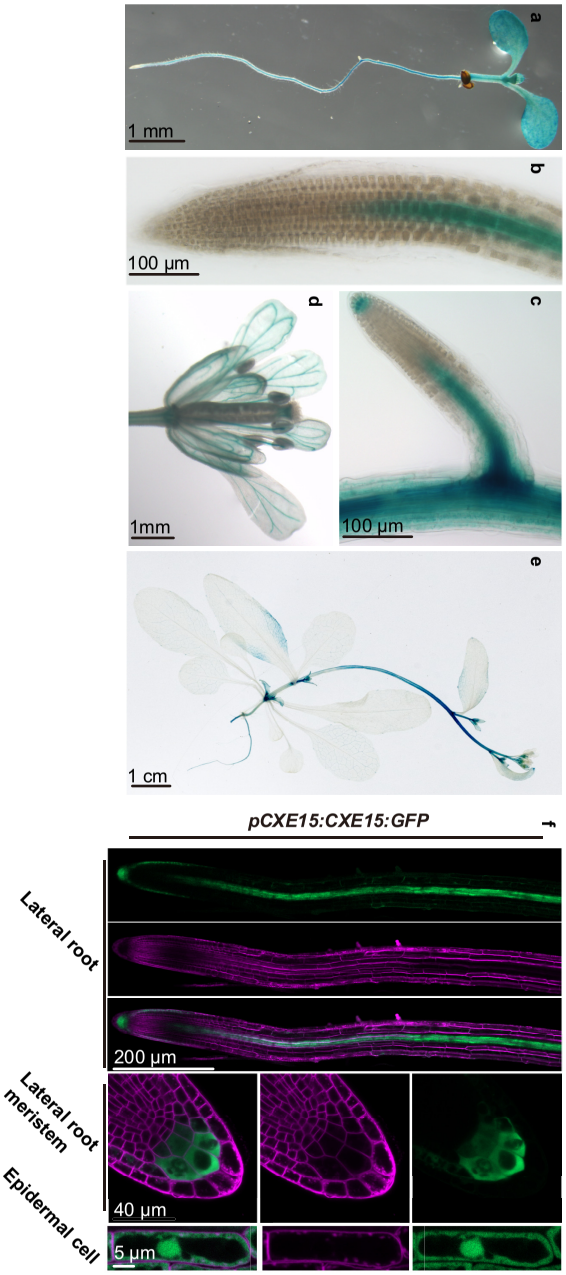
a
1 mm
b
100 µm
d
1mm
c
100 µm
e
1 cm
pCXE15:CXE15:GFP
f
Lateral root
200 µm
Lateral root meristem
40 µm
Epidermal cell
5 µm

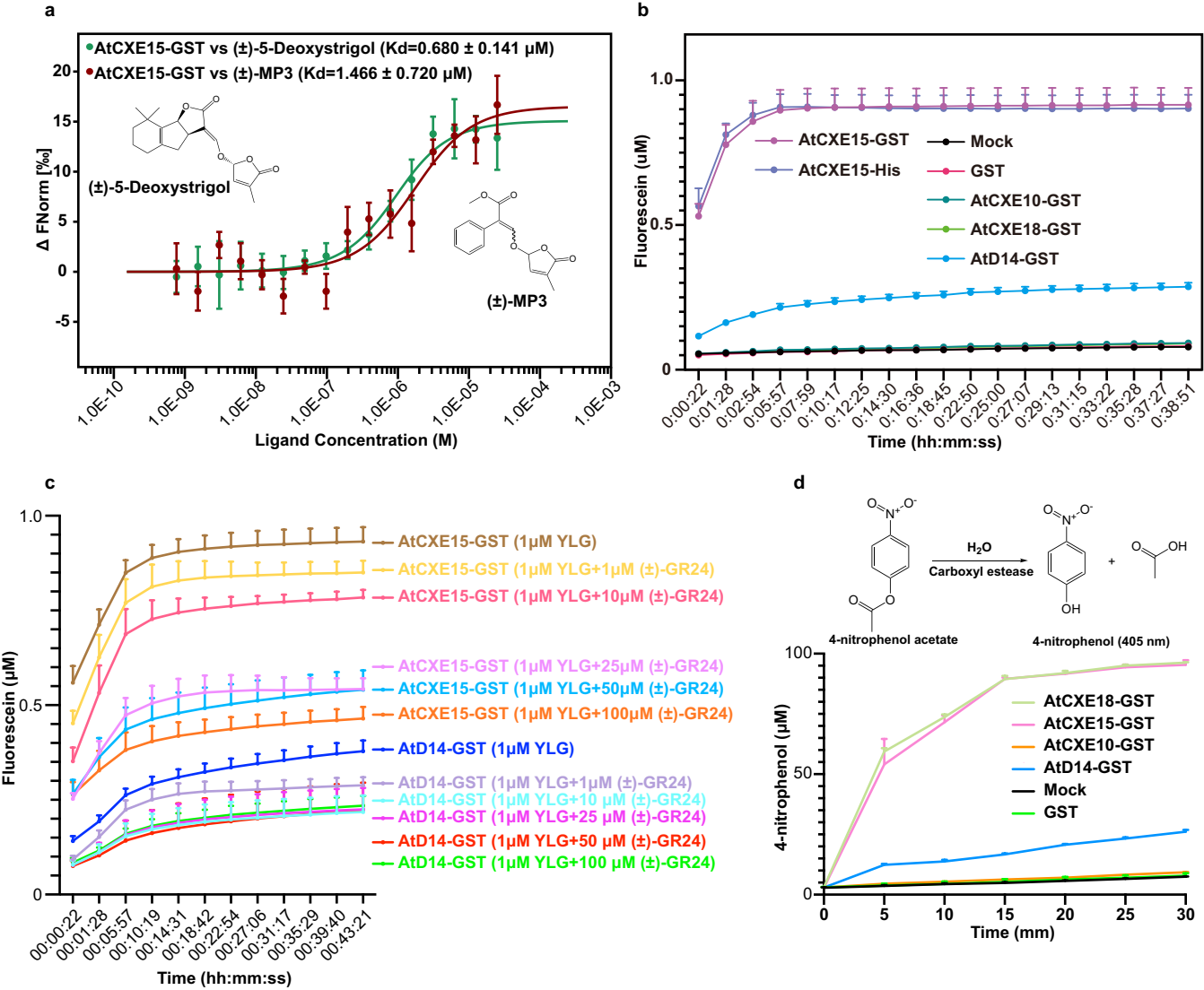
a
AtCXE15-GST vs (±)-5-Deoxystrigol (Kd=0.680 ± 0.141 μM)
AtCXE15-GST vs (±)-MP3 (Kd=1.466 ± 0.720 μM)
(±)-5-Deoxystrigol
(±)-MP3
Δ FNorm [‰]
Ligand Concentration (M)
b
AtCXE15-GST
AtCXE15-His
Mock
GST
AtCXE10-GST
AtCXE18-GST
AtD14-GST
Fluorescein (uM)
Time (hh:mm:ss)
c
AtCXE15-GST (1μM YLG)
AtCXE15-GST (1μM YLG+1μM (±)-GR24)
AtCXE15-GST (1μM YLG+10μM (±)-GR24)
AtCXE15-GST (1μM YLG+25μM (±)-GR24)
AtCXE15-GST (1μM YLG+50μM (±)-GR24)
AtCXE15-GST (1μM YLG+100μM (±)-GR24)
AtD14-GST (1μM YLG)
AtD14-GST (1μM YLG+1μM (±)-GR24)
AtD14-GST (1μM YLG+10 μM (±)-GR24)
AtD14-GST (1μM YLG+25 μM (±)-GR24)
AtD14-GST (1μM YLG+50 μM (±)-GR24)
AtD14-GST (1μM YLG+100 μM (±)-GR24)
Fluorescein (μM)
Time (hh:mm:ss)
d
H2O
Carboxyl estease
4-nitrophenol acetate
4-nitrophenol (405 nm)
AtCXE18-GST
AtCXE15-GST
AtCXE10-GST
AtD14-GST
Mock
GST
4-nitrophenol (μM)
Time (mm)

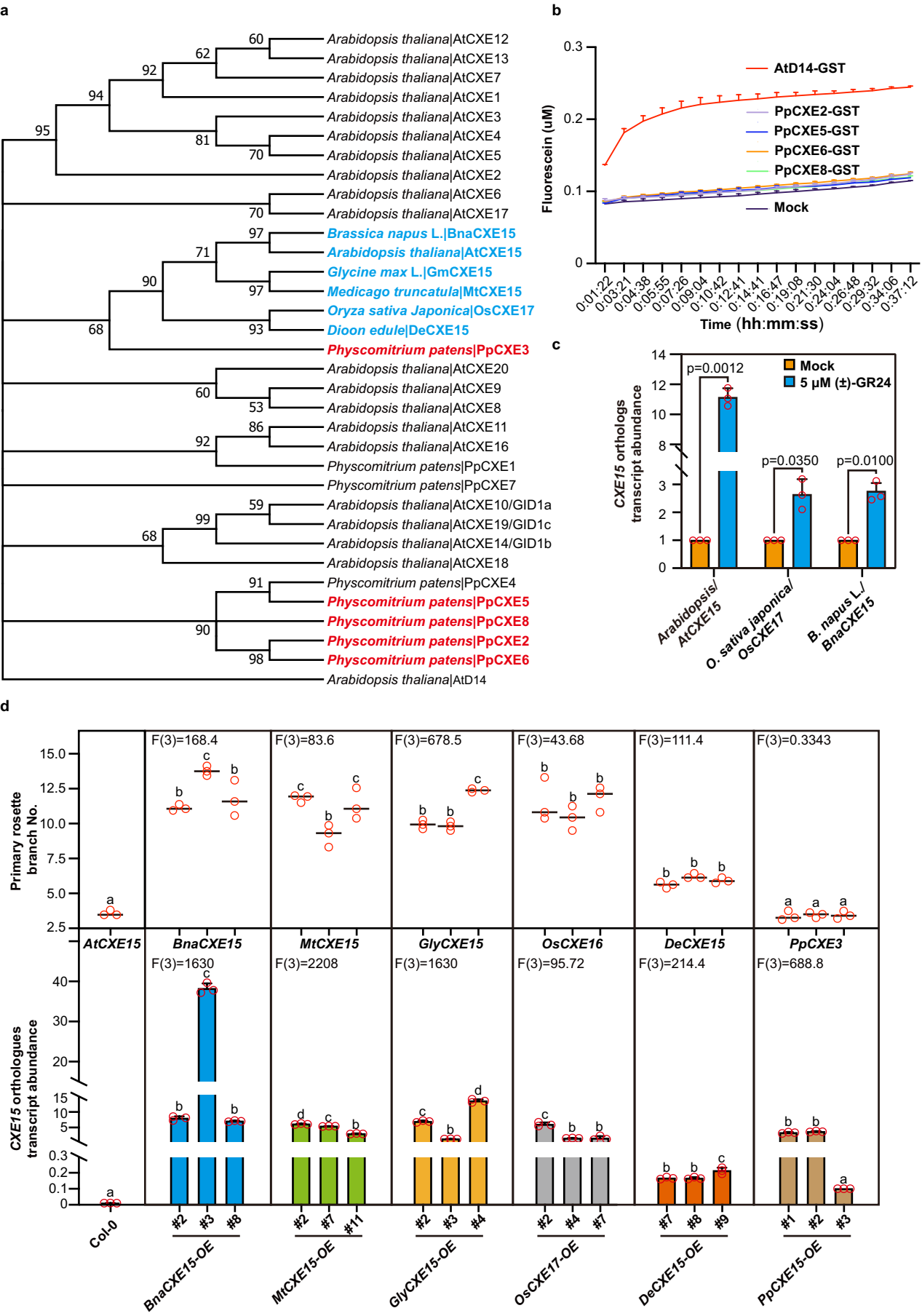
a
Arabidopsis thaliana|AtCXE12
Arabidopsis thaliana|AtCXE13
Arabidopsis thaliana|AtCXE7
Arabidopsis thaliana|AtCXE1
Arabidopsis thaliana|AtCXE3
Arabidopsis thaliana|AtCXE4
Arabidopsis thaliana|AtCXE5
Arabidopsis thaliana|AtCXE2
Arabidopsis thaliana|AtCXE6
Arabidopsis thaliana|AtCXE17
Brassica napus L.|BnaCXE15
Arabidopsis thaliana|AtCXE15
Glycine max L.|GmCXE15
Medicago truncatula|MtCXE15
Oryza sativa Japonica|OsCXE17
Dioon edule|DeCXE15
Physcomitrium patens|PpCXE3
Arabidopsis thaliana|AtCXE20
Arabidopsis thaliana|AtCXE9
Arabidopsis thaliana|AtCXE8
Arabidopsis thaliana|AtCXE11
Arabidopsis thaliana|AtCXE16
Physcomitrium patens|PpCXE1
Physcomitrium patens|PpCXE7
Arabidopsis thaliana|AtCXE10/GID1a
Arabidopsis thaliana|AtCXE19/GID1c
Arabidopsis thaliana|AtCXE14/GID1b
Arabidopsis thaliana|AtCXE18
Physcomitrium patens|PpCXE4
Physcomitrium patens|PpCXE5
Physcomitrium patens|PpCXE8
Physcomitrium patens|PpCXE2
Physcomitrium patens|PpCXE6
Arabidopsis thaliana|AtD14
b
Fluorescein (uM)
AtD14-GST
PpCXE2-GST
PpCXE5-GST
PpCXE6-GST
PpCXE8-GST
Mock
Time (hh:mm:ss)
c
CXE15 orthologs transcript abundance
Mock
5 μM (±)-GR24
p=0.0012
p=0.0350
p=0.0100
Arabidopsis/ AtCXE15
O. sativa japonica/ OsCXE17
B. napus L./ BnaCXE15
d
Primary rosette branch No.
F(3)=168.4
F(3)=83.6
F(3)=678.5
F(3)=43.68
F(3)=111.4
F(3)=0.3343
AtCXE15
BnaCXE15
MtCXE15
GlyCXE15
OsCXE16
DeCXE15
PpCXE3
CXE15 orthologues transcript abundance
F(3)=1630
F(3)=2208
F(3)=1630
F(3)=95.72
F(3)=214.4
F(3)=688.8
Col-0
BnaCXE15-OE
MtCXE15-OE
GlyCXE15-OE
OsCXE17-OE
DeCXE15-OE
PpCXE15-OE

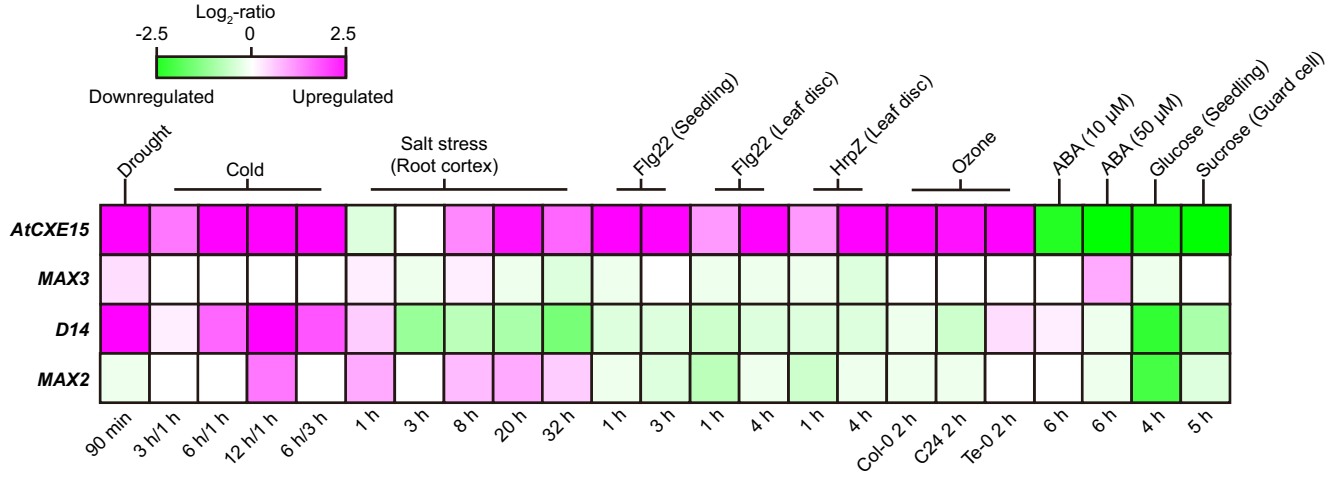
Log2-ratio
-2.5
0
2.5
Downregulated
Upregulated
Drought
Cold
Salt stress (Root cortex)
Flg22 (Seedling)
Flg22 (Leaf disc)
HrpZ (Leaf disc)
Ozone
ABA (10 µM)
ABA (50 µM)
Glucose (Seedling)
Sucrose (Guard cell)
AtCXE15
MAX3
D14
MAX2
90 min
3 h/1 h
6 h/1 h
12 h/1 h
6 h/3 h
1 h
3 h
8 h
20 h
32 h
1 h
3 h
1 h
4 h
1 h
4 h
Col-0 2 h
C24 2 h
Te-0 2 h
6 h
6 h
4 h
5 h